Surv Geophys (2007) 28:199–237
DOI 10.1007/s10712-007-9023-x

ORIGINAL PAPER

# EM Monitoring of Crustal Processes Including the Use of the Network-MT Observations

**Makoto Uyeshima**

Received: 17 January 2007 / Accepted: 21 June 2007


**Abstract** There are several kinds of coupling mechanisms which can convert mechanical, chemical or thermal energies due to seismic or volcanic activities into electromagnetic energies. As a result of concentrated efforts in laboratory and theoretical research, the basic relationship between the intensity of electromagnetic sources and changes in mechanical, chemical and thermal state is becoming established. Also with the progress of the electromagnetic simulation techniques, it has been possible to evaluate in situ sensitivity. Based on this progress and also due to extensive improvement in measuring techniques, many field experiments have been performed to elucidate subsurface geophysical processes underlying the preparation stage, onset, and subsequent healing stage of earthquakes and volcanic eruptions. In volcanic studies, many studies have reported the measurement of electromagnetic signals which were successfully interpreted in terms of various driving mechanisms. Although there have been numerous reports about the existence of precursory electromagnetic signals in seismic studies, only a few of them could be successfully explained by the proposed mechanisms, whereas coseismic phenomena are often consistent with those mechanisms including the absence of detectable signals. In many cases, one or two orders of higher sensitivity were required, especially for precursory signals. Generally, electromagnetic methods are more sensitive to near-surface phenomena. It will be necessary to discriminate electromagnetic signals due to these near-surface sources, which often possess no relationship with the crustal activities. Further efforts to enhance in situ sensitivity through improvements in observation techniques and in data processing techniques are recommended. At the same time, multi-disciplinary confirmation against the validity of electromagnetic phenomena will inevitably be necessary. A Network-MT observation technique has been developed to determine large-scale deep electrical conductivity structure. In the method, a telephone line network or purpose-built long baseline cables are utilized to measure voltage differences with long electrode separations. Because of the averaging effect of the electric fields, static shift problems due to small-scale, near-surface lateral heterogeneities can be alleviated. Several field experiments revealed regional scale deep electrical conductivity structures related to slab subduction or its

M. Uyeshima (✉)
Earthquake Research Institute, The University of Tokyo, 1-1-1 Yayoi, Bunkyo, Tokyo 113-0032, Japan
e-mail: uyeshima@eri.u-tokyo.ac.jp

stagnation, which enable us to elucidate underlying physical processes caused by the slab motion. The technique can also be applied to monitor the electric potential field related to crustal activities. The annual variation of the potential field and electrical conductivity in the French Alps were interpreted to be caused by the annual variation of lake water level. The method was also used to monitor the regional scale spatio-temporal variation of the SP field and electrical conductivity before and at the onset of earthquakes and volcanic eruptions.

**Keywords** Electromagnetic methods · Earthquake · Volcano · Monitoring · Network-MT method

## 1 Introduction

Electromagnetic methods have long been applied to elucidate underlying geophysical mechanisms in seismic activity or volcanic eruptions, to monitor or to predict them. This is because electromagnetic methods possess the potential to detect temporal variations of underground geophysical states such as temperature, strain, stress and the existence, flow, salinity and connectivity of subsurface fluids, with the aid of resistivity, electrokinetic effects, thermal magnetic effects, piezo-electromagnetism and other solid state charge generation mechanisms. The time scales of EM temporal variations are primarily dependent on the time scales of the relevant geophysical mechanisms that drive the respective EM disturbances. Accumulation of stress and strain between main shocks or main volcanic eruptions, and variation of temperature due to thermal conduction are rather slow processes whose time scales are longer than years. Time scales of stress–strain variations due to the intrusion of magma before volcanic eruption or nucleation just before a main shock are from hours to several days. Variations of temperature or of the content of interstitial fluids due to the movement of fluids possess similar time scales. Coseismic phenomena including the generation of fracture or co-eruptive phenomena take place on a more rapid time scale, shorter than hours. Another factor in the determination of time scales of EM disturbances is the dissipation of EM waves in the conducting earth. Even if rapid phenomena occur in a very deep part of the earth, EM disturbances cannot reach the earth's surface due to the Joule losses. Electric (or SP) field monitoring is useful in deriving information related to electric sources such as piezoelectricity, other solid state charge generation mechanisms, electrokinetic phenomena, and the variation of electrical conductivity. From magnetic field monitoring, we can derive information related to magnetic sources and the distribution of electric current, such as thermal magnetic effects, piezomagnetic phenomena, electrokinetic phenomena, and electrical conductivity. Electromagnetic field monitoring can afford us information about electromagnetic waves that are generated in the earth and can be propagated to the surface, besides information related to electrokinetic phenomena and variation of electrical conductivity. Another category of electromagnetic monitoring is based on a variety of controlled source EM methods, which are mainly useful in monitoring variations in the electrical conductivity structure.

After several key observations of electromagnetic phenomena, e.g. ULF emissions at great Chilean and Loma Prieta earthquakes (Warwick et al. 1982; Fraser-Smith et al. 1990), resistivity variations in China and Japan (e.g. Yamazaki 1975; Zhao and Qian 1994; Chu et al. 1996), SP anomaly and variations at the La Fournaise and Unzen volcanoes (Zlotnicki et al. 1994; Hashimoto and Tanaka 1995), seismic electric signals (SES) in Greece (Varotsos and Alexopoulos 1984a, b), the importance of the electromagnetic

monitoring captured the attention in the world-wide geophysical community, even though some of the phenomena are still debatable, and several big projects were established. These key observations were summarized in previous review papers (Park et al. 1993; Park 1996; Johnston 1997) and later, many contributions reporting the results of the projects were published in several proceedings or special issues (e.g. Hayakawa 1999; Biagi et al. 2000; Hayakawa and Molchanov 2002; Uyeda and Park 2002; Hayakawa et al. 2004; Parrot 2006; Harinarayana and Zlotnicki 2006), as well as in independent research papers.

In this article, I review recent progress in EM-monitoring research. There are several different kinds of driving mechanisms which can be monitored electromagnetically. I shall review the contributions based on these respective driving mechanisms. Although there have been many papers reporting precursory electromagnetic radiations in a rather high frequency range (higher than the ELF bands) together with precursory ionosphere-terrestrial coupling, I will not describe them in detail here, since not all of their driving mechanisms have been clarified yet. Concerning these phenomena, the reader is referred to contributions in the proceedings or the special issues listed above. After the EM-monitoring research, I will briefly introduce the Network-MT observation technique, where long baseline telluric measurements are performed by using a telephone line network. The technique can be used both to determine regional scale deep electrical conductivity structure and the spatial distribution of the telluric potentials, and to monitor their temporal variation.

## 2 EM Monitoring

### 2.1 General Considerations

Macroscopic electromagnetic fields in a conductive substance are described by Maxwell's equations in the form,

$$\nabla \times \vec{H} = \frac{\partial \vec{D}}{\partial t} + \sigma \vec{E} + \vec{i}_s \tag{1a}$$

$$\nabla \times \vec{E} = -\frac{\partial \vec{B}}{\partial t} \tag{1b}$$

$$\nabla \cdot \vec{B} = 0 \tag{1c}$$

$$\nabla \cdot \vec{D} = \rho_e, \tag{1d}$$

where $\vec{H}$, $\vec{B}$, $\vec{E}$, $\vec{D}$, and $\rho_e$ represent magnetic field, magnetic induction, electric field, electric displacement, and electric charge density, respectively. In Ampere's law (Eq. 1a), the source electric current $\vec{i}_s$ and the electrical conductivity $\sigma$ are related to the subsurface thermal, mechanical and chemical properties or their temporary variations through their respective coupling relationships, as will be seen in Sect. 2.2. If some source electric current is generated in the earth, some associated variation of the electromagnetic fields will occur. If the electrical conductivity structure varies, some variation in the electromagnetic responses will be expected. Thus what we should do in electromagnetic monitoring is first detect such electromagnetic field or response variations, and then estimate the spatial and temporal variation of the respective subsurface

electromagnetic sources or the electrical conductivity structure. The ultimate goal is to elucidate the variation of subsurface thermal, mechanical and chemical properties. Since dissipation due to conducting currents plays a main role in estimating electromagnetic wave propagation in the earth, determination of the electrical conductivity structure is also very important.

In ideal cases, we can uniquely estimate the spatio-temporal distribution of the source currents merely from the electromagnetic observations. Although this has not been realized yet, a candidate for the ideal case in the future will be determination of electrical conductivity structure such as that in Utada (2003). In most of the actual experiments, however, the number of sites and the acquired frequency range are often insufficient for such a direct estimation. As in the case of the potential problem in static problems, we cannot uniquely determine the source current solely from surface observations (e.g. Blakely 1995). In some cases we do not know whether observed electromagnetic disturbances are truly related to crustal activities (e.g. Pham et al. 1998, 1999, 2001, 2002; Utada et al. 1998, 2000). Thus normally we first make a thermal or mechanical model to estimate, for example, the stress distribution based on a specific fault model, as in piezomagnetic investigations reviewed by Sasai (1994, 2001). Next, the corresponding electromagnetic source and electromagnetic fields at the observation sites are estimated. By comparing synthetic and observed fields, we can derive the parameters of the fault model in the above piezomagnetic studies, and can also guarantee that the observed field really is caused by certain crustal activities. When some electromagnetic sources are generated by crustal activities, the resultant electromagnetic field must, in turn, affect the crustal activities at the same time. In most of the cases, however, such electromagnetic osmotic forces are much weaker than the mechanical forces that drive the original crustal activities. Then the forward modeling becomes kinematic. Kinematic modeling is exactly the same as modeling in controlled source prospecting. In modeling controlled source problems, the source current $i_s$ in Ampere's law in Eq. 1a is a specified artificial current.

## 2.2 Electromagnetic Sources

### *2.2.1 Magnetic Polarization (Magnetization)*

*Thermal Magnetic Effects*. A ferromagnetic or ferrimagnetic substance, such as iron or magnetite, is characterized by its spontaneous magnetization. As the temperature is increased, its magnetization is eventually lost at the Curie temperature. The Curie temperature of magnetite is 580°C. When igneous rocks with such magnetic minerals are cooled down below the Curie temperature, they acquire magnetization parallel to the geomagnetic field at that time. This temperature dependence of the magnetization was investigated long ago and its physical mechanism was also well established (e.g. Nagata 1943; Néel 1949; Merrill et al. 1996). Subsurface temperature variations, especially in volcanic areas, can produce geomagnetic temporal variations due to this thermal magnetic effect.

Since the change of temperature field is rather slow (from days to years), the problem is treated as static. The magnetic field is irrotational and is described by a magnetic potential. The magnetic field $\vec{H}(\vec{x}, t)$ at an observation point $\vec{x}$ at time $t$, due to a spatial distribution of the magnetization $\vec{M}(\vec{x}', t)$, is expressed as

$$\vec{H}(\vec{x},t) = -\nabla \int_V \vec{M}(\vec{x}',t) \frac{(\vec{x}-\vec{x}')}{4\pi\left|\vec{x}-\vec{x}'\right|^3} dV', \tag{2}$$

where $\vec{M}(\vec{x}',t)$ is defined as

$$\vec{M}(\vec{x}',t) = \chi(\vec{x}',t)\vec{H}(\vec{x}',t) + \vec{M}_s(\vec{x}',t). \tag{3}$$

The first and second terms of the right-hand side of Eq. 3 are, respectively, induced and spontaneous magnetization. $\chi$ is the magnetic susceptibility. Equation 2 can be also recognized as evaluating the temporal variation of the magnetic field $\vec{H}(\vec{x},t)$ due to the variation of the magnetization $\vec{M}(\vec{x}',t)$. Generally speaking, we cannot uniquely determine the source in the potential problem (e.g. Blakely 1995). In practical applications, magnetization is assumed to be uniformly distributed in some elementary shape such as a sphere (equivalent to a single magnetic dipole), a cylinder, a prism or their aggregates. Then its depth position, its size and the intensity of the magnetization variation are determined. Temperature variation is estimated from these model parameters by referring to the temperature dependence of the magnetization (e.g. Tanaka 1993; Del Negro and Ferrucci 1998, 2000; Sasai et al. 2001a, b; Hurst et al. 2004). As an example, temporal variations of the geomagnetic total force intensity prior to the 2000 Miyake-jima volcanic island eruption, Japan, is shown in Fig. 1 (Sasai et al. 2001a). The eruption started on June 26, 2000 with swarm activity near the summit. Subsequently, a large sinkhole was suddenly formed at the summit area on July 8, and a series of major summit eruptions took place during July and August. After that, a large amount of $SO_2$ gas was emitted from the summit, which forced local people to evacuate the island. At OYM station close to the summit, the total intensity continued to increase from the middle of 1996, whereas at TRK about 2 km south of OYM, the total intensity decreased. At other stations, there were almost no temporal variations. These total intensity variation indicated that thermal demagnetization took place about 700 m beneath between OYM and TRK. The radius of the demagnetized sphere is estimated to be 130 m if perfect demagnetization ($T > 580°C$ by magma) is assumed, and to be 280 m if partial demagnetization ($\Delta T \sim 100°C$ by hydrothermal activity) is assumed. Similarly, the movement, extinction and generation of the magnetic body can also be sensed by geomagnetic observations. Prior to and during the generation of the sink hole on July 8, an intense magnetic field variation was observed. This is because the magnetized body was crushed or replaced by air. On the other hand, a formation of magnetic particles and/or magnetization during faulting or due to thunder strikes has been reported (e.g. Enomoto and Zheng 1998; Nakamura et al. 2002; Fukuchi 2003; Verrier and Rochette 2002). Moreover, the remanent magnetization provides a means of determining the electric current intensity of a thunder strike or the amplitude of electric phenomena during faulting (e.g. Verrier and Rochette 2002; Enomoto and Zheng 1998; Ferré et al. 2005).

Another example concerns the cooling history of the dike at Mt. Etna, Italy after the major eruption between September 11 and October 9, 1989 (Del Negro and Ferrucci 1998). From October 23, just after the cessation of the eruption, repeated total force intensity surveys along the same profile across the fracture at the SSE foot of Mt. Etna were performed for 2 years. Until March 1990, there were no significant magnetic changes. However, after a small anomaly of about 30 nT was first observed at the fracture on July 4, 1990, the intensity of the anomaly gradually grew and finally reached 130 nT on June 8, 1991. After that, no significant variation was observed until September 1991. In order to

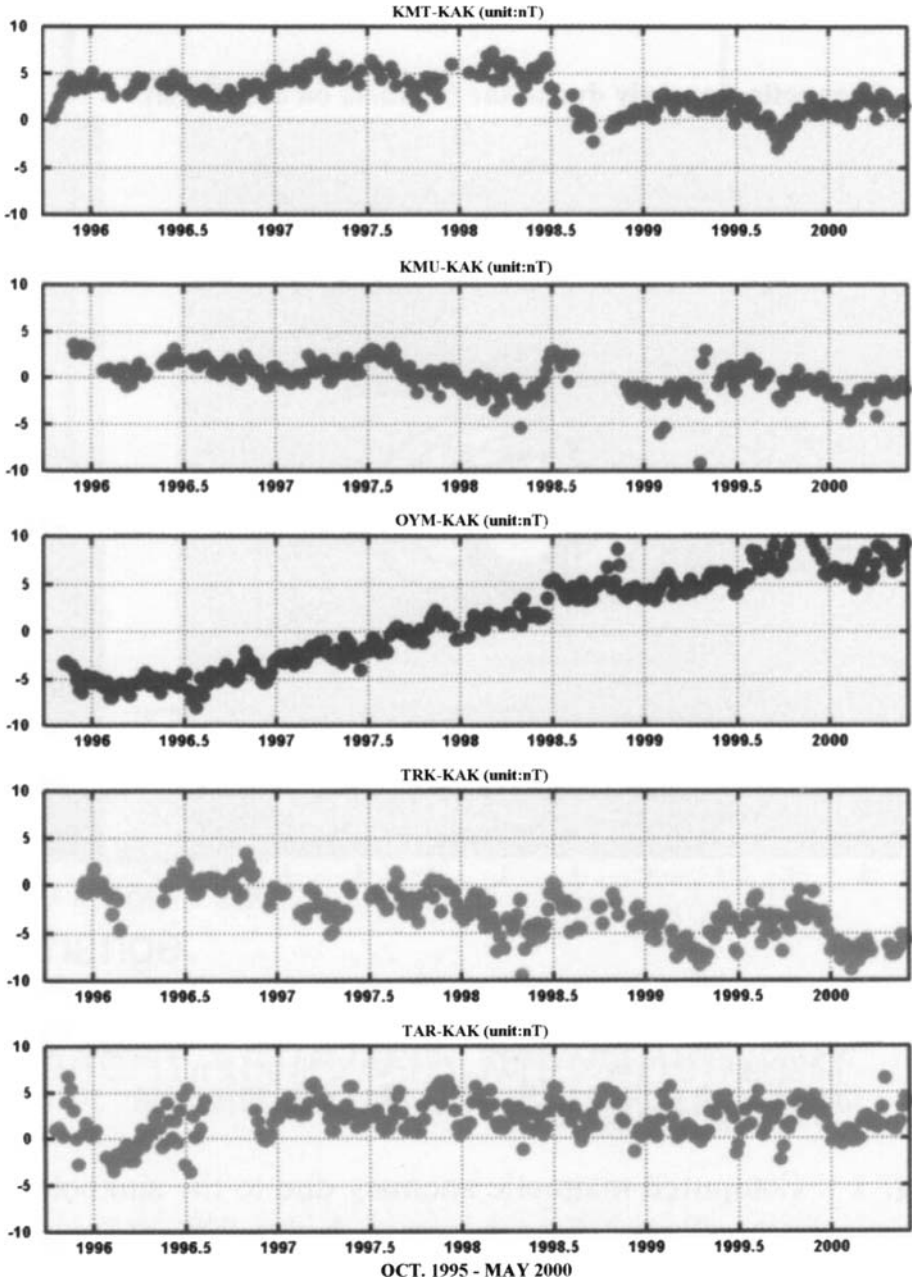


**Fig. 1** Changes in magnetic total force intensity at stations along the central N–S line on Miyake-jima island, central Japan. Five-day means of simple differences relative to Kakioka geomagnetic observatory, JMA, are plotted (Sasai 2001a)

explain this spatio-temporal total force change, the authors devised a model of the cooling dyke which gradually acquired magnetization, as shown in Fig. 2. The model shows that the dike acquired 25 and 50% magnetization on July 4, 1990 and September 23, 1990,

respectively. The magnetizations correspond, respectively, to 380°C and to 240°C. Thus they confirmed that magma intrusion occurred even at the SSE flank of Mt. Etna, where no gaseous emission was observed on the surface. The magnetization model shown in Fig. 2 was refined later by a sophisticated inversion scheme using the genetic algorithm (Currenti et al. 2005).

Magnetic total force records often contain annual variations. This annual variation is characterized by a diversity of amplitude, phase and polarity from site to site even in one target region. Thus, this variation is likely to be caused by local or near-surface sources. In order to test whether this variation is the result of a small fluctuation of local magnetization due to the annual temperature variation, Utada et al. (2000) conducted a local geomagnetic

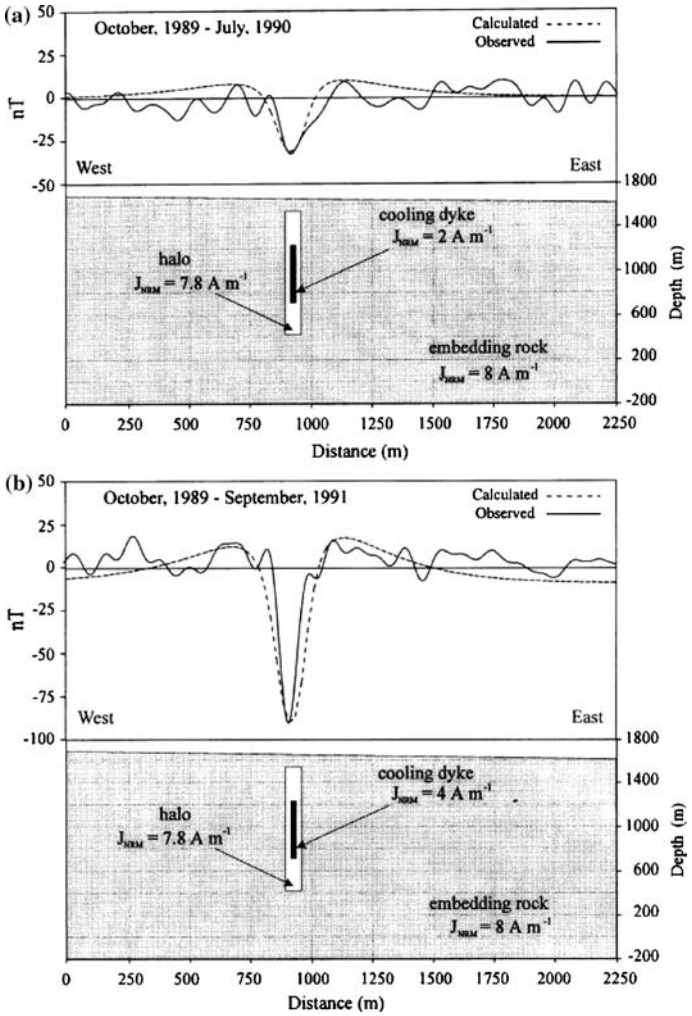


**Fig. 2** Spatial distribution of total force intensity change (upper) and its thermomagnetic model of dyke (lower) on (**a**) Jul. 4, 1990, and (**b**) on Sep. 23, 1990. In the upper panel, observed change (solid line) is compared with calculated change from the model in the lower panel (broken line) (Del Negro and Ferrucci 2000)

survey around various sites. At sites located on a relatively positive anomaly, the total force tends to decrease in summer, whereas at sites located on a relatively negative anomaly, it tends to increase in summer. This fact strongly suggests that the annual variation is caused by near-surface thermal magnetic effects, since a local magnetic anomaly tends to fade as temperature increases. Since the spatial wavelength of the magnetic anomaly corresponds to the depth of the magnetized body causing the geomagnetic anomaly at the surface, phase variation is also explained by a downward thermal diffusion process and the depth of the magnetized body which controls the local magnetic anomaly. This annual variation is sometimes seen as an obstacle when interpreting the monthly variation of the total force. Thus temperature measurements at respective magnetic sites are now desirable and it is necessary to remove this effect before interpretation (e.g. Del Negro and Currenti 2003; Hashimoto et al. 2003).

In addition to the conventional thermal magnetic effects described above, a sharp increase in magnetic susceptibility at temperatures just below the Curie temperature (the so-called Hopkinson peak (Hopkinson 1889)) will be another source for EM monitoring studies. As Kiss et al. (2005) argued, the magnetic permeability increase just below the Curie temperature is caused by the second order magnetic phase transition, which, on the basis of the theory and recent experiments referred to in the paper, is one or two orders of magnitude greater than the normal permeability for igneous rocks with high magnetite contents. If this enhancement is relevant in the real earth, conventional interpretations of magnetotelluric soundings and magnetization mappings should be re-interpreted in terms of this increasing permeability. In addition, since the thickness of the layer with high permeability and its intensity are controlled by the thermal state of the layer just below the Curie temperature, we will also be able to monitor variation of the thermal state by monitoring the depth of the layer, its thickness and intensity, especially in the volcanic fields.

*Piezomagnetic Effects*. Another mechanism which alters the magnetization is the piezomagnetic effect where changes in subsurface stress cause changes in magnetization. The piezomagnetic effect in rocks was discovered in the 1950's (e.g. Kalashnikov and Kapitsa 1952). Basic experimental results on the stress-magnetization relationship were summarized by Nagata (1970). For reversible changes, piezomagnetization is proportional to stress below a few 10 MPa. As with the thermal magnetic effect, when the time scale of the physical process under investigation is very long (hours to years), as with stress accumulation related to slab subduction or fluid intrusion, or in the intervals before and after coseismic fault motions, we can treat the problem as static. Hence, exactly the same formula as Eq. 2 can also be applied to the piezomagnetic problems (e.g. Stacey 1964). The piezomagnetic magnetization variation $\Delta\vec{M}$ is expressed as,

$$\Delta\vec{M} = \frac{3}{2}\beta\vec{\vec{T}}'\vec{M}, \tag{4}$$

where $\vec{\vec{T}}'$ and $\vec{M}$ are the deviatric stress tensor and original magnetization with no stress (Sasai 1980; Hao et al. 1982). The coefficient $\beta$ is called the stress sensitivity and typically has an order of $10^{-3}$ $\mathrm{MPa}^{-1}$. The most generalized piezomagnetic constitutive law should include the full stress tensor as was proposed by Zlotnicki et al. (1981). Equation 4 is valid only in a special case of an isotropic medium (Sasai 1980), which, however, explains the results from laboratory experiments well (e.g., Nagata 1970).

Solutions for the elastic field due to elementary mechanical sources in an elastic half space, such as a point dilatation source (Mogi model; Mogi 1958), or a point dislocation

source (Maruyama 1964), have been obtained analytically. Hence we can estimate the magnetic field variation due to such mechanical sources by using a linear piezomagnetic relationship (Eq. 4) and the integral Eq. 2. Although the solution for stress-induced magnetization involves a singularity which is difficult to treat, Sasai (1991) finally obtained accurate solutions to the integral Eq. 2. The road to the accurate solutions and their applications are summarized in a review paper by Sasai (1994). Subsequent progress in modeling techniques such as the inclusion of 2-D topography (Sakanaka et al. 1997), or generalization of the fault model (based on the stress field of an inclined strike-slip, or dip-slip or tensile fault (Okada 1992)) by Utsugi et al. (2000), are reviewed in Sasai (2001). The effects of non-uniform elasticity were investigated in Okubo and Oshiman (2004).

The advantage of piezomagnetic research is that it is almost the only way to probe the spatial distribution of the subsurface stress changes directly, and that it enables us to compare the elastic source parameters with those derived from geodetic and seismic studies. Once accurate solutions have been derived, researchers can use them to elucidate elastic source mechanisms due to magma intrusions or volcanic inflations (Sasai et al. 2002; Del Negro and Currenti 2003; Del Negro et al. 2004; Currenti et al. 2005). In seismic research, the method is used to monitor preseismic stress accumulation and its fluctuation, and to determine coseismic stress change (Johnston et al. 1994; Stuart et al. 1995; Sasai and Ishikawa 1997; Nishida et al. 2004).

Since the magnetization of igneous rocks can be up to 10 A/m, a fairly large amplitude of magnetic field change of piezomagnetic origin can also be expected due to the relatively shallow locations of the mechanical sources. Del Negro et al. (2004), for example, recorded up to 10 nT temporal variations accompanying the onset of the 2002–2003 volcanic eruptions of Mt. Etna, Italy. However, the magnetization in areas with seismic activity is often ten times smaller than that of volcanoes. In addition, the location of a seismic fault for a main shock cannot normally be predicted exactly before the onset of the main shock, whereas the position of a volcanic eruption can be predicted more accurately from the history of volcanic eruptions. Furthermore, the epicenter is normally much deeper than the depth of magma intrusions. Even the detection of coseismic piezomagnetic signals is much more difficult than with volcanic eruptions. Since uniform magnetization in a layer produces no net magnetic field on the surface (e.g. Blakely 1995), it is the spatial variation of the magnetization and/or stress field that produces the observable magnetic field on the surface (Banks et al. 1991). Thus the magnetic field variation on the surface is confined near the edges of the seismic faults where significant spatial variations of stress exists, and/or near the edges of the magnetized body. Even for the Landers earthquake of Mw 7.3 in 1992, for example, the coseismic geomagnetic variation is only about 1 nT within 20–30 km of the seismic fault. This coseismic change was well reproduced by the synthetic model of Johnston et al. (1994).

Several large geomagnetic secular variations of order 1 nT/year have been reported, however, which are possibly due to stress accumulation accompanying a subduction process. Nishida et al. (2004) detected such a temporal variation as long as 30 years in Hokkaido, at the SW end of the Kuril Arc, as shown in Fig. 3. They examined whether this variation could be explained by the piezomagnetic effect. Since some of the stations are located on a significantly magnetized body and the spatial variation can cause a magnification of the temporal variation of the piezomagnetic field, they first determined the magnetization structure by performing a detailed magnetic survey of the area. Then, based on the magnetization structure, they estimated spatio-temporal variation of the synthetic surface field due to an estimated uniform strain accumulation of $4 \times 10^{-7}$/year based on geodetic surveys (Ishikawa and Hashimoto 1999). As a result, the stress sensitivity of

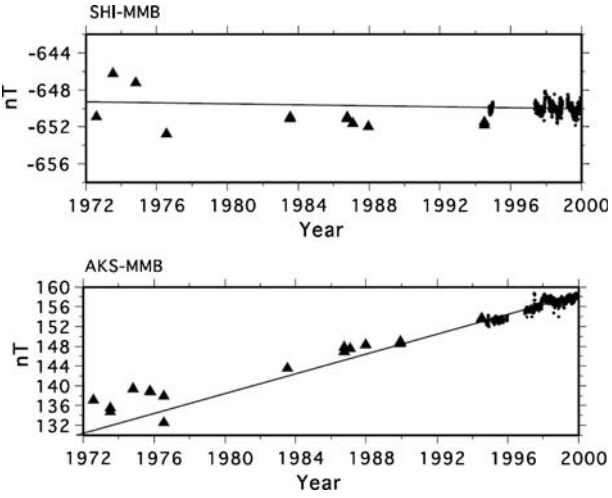


**Fig. 3** Temporal changes of the total force intensity at AKS and SHI (reference: Memambetsu geomagnetic observatory, JMA). The changes obtained by repeated measurements are shown by solid triangles, while whole-day mean simple differences calculated from the continuous monitoring records are plotted by solid circles. Linear least-squares regression lines applied for the periods from August 1996 to November 1999 are extrapolated to 1972 (Nishida et al. 2004)

$10^{-2}$ MPa, one order higher than normal sensitivity, was necessary to explain the spatio-temporal distribution of the observed magnetic field (Fig. 4). A similar discrepancy is also detected in research aimed at determining the in-situ stress sensitivity using the loading variation due to seasonal change of water level in artificial lakes (e.g. Davis and Stacey 1972; Abdullabekov et al. 1979; Brenan and Hastie 1979; Zhan 1989; Oshiman et al. 1991). Although stress sensitivity is high for some porous rocks (Hamano 1983), those rocks are not commonly distributed. Further research will be necessary to explain this enigma. A key seems to lie in the time scale of the deformation, since coseismic changes and rather rapid changes near volcanoes are well explained by the stress sensitivity determined from laboratory experiments, whereas a higher sensitivity is necessary to reproduce the secular variation.

### 2.2.2 *Electric Polarization*

*Piezoelectric Effects*. Piezoelectricity is caused by an asymmetric lattice structure in some rock forming minerals such as quartz. Due to the asymmetric lattice orientation, a temporal stress variation alters the electrical polarization of those minerals. In the theory of linear piezoelectricity, the electric polarization $\vec{P}$ is expressed as

$$\vec{P} = \overleftrightarrow{d}\vec{T}, \tag{5}$$

where $\vec{T}$ is a vector composed of six independent components of the stress tensor and $\overleftrightarrow{d}$ represents the piezoelectric coefficients expressed by a $3 \times 6$ matrix, which characterizes the symmetry type of the medium (e.g. Ikeda 1990). Equation 5 includes all the components of the full stress tensor, which is different from the piezomagnetic case (Eq. 4). The electric polarization, however, also vanishes under hydrostatic pressure for many kinds of crystals, including quartz, or aggregates of piezoelectric crystals with specific symmetries.

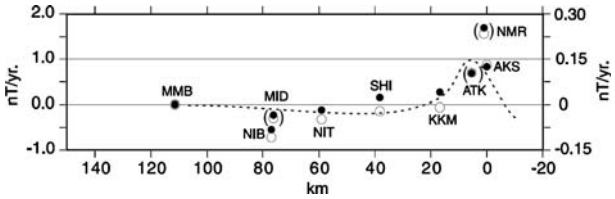


**Fig. 4** Observed secular changes (open circles) and corrected ones for the orientation effect (Davis and Johnston 1983, solid circles) are plotted against the horizontal distance from AKS to MMB. Amplitudes are referred to the left-side ordinate. For convenience of comparison, the values at NMR, ATK and MID are also projected onto the measurement line. Calculated piezomagnetic field is shown by a dashed curve (right-side ordinate). Both the stress sensitivity of remanence and susceptibility are assumed to be $2 \times 10^{-3}$ $MPa^{-1}$ for the calculation (Nishida et al. 2004)

Although a typical magnitude of the elements of the piezoelectric coefficient matrix for a single crystal quartz is $10^{-12}$ (C/N), that of a quartzite (aggregates of quartz) is typically $10^{-15}$ (C/N) due to the cancellation effect of the rather randomly oriented crystal axes that control the piezoelectricity (e.g. Tuck et al. 1977; Bishop 1981). Since the electric displacement D is written by

$$\vec{D} = \varepsilon \vec{E} + \vec{P}, \tag{6}$$

an effective external current source term $\vec{i}_s^{\,p.e.}$ in Ampere's law (Eq. 1a) due to piezoelectricity is expressed by

$$\vec{i}_s^{\,p.e.} = \overleftrightarrow{d} \frac{\partial \vec{T}}{\partial t}. \tag{7}$$

Piezoelectricity was considered to be a leading mechanism to explain the coseismic or even preseismic electromagnetic phenomena (e.g. Nitsan 1977; Warwick et al. 1982). Laboratory experiments to monitor electromagnetic potential changes associated with the stick-slip events of dry granite (Yoshida et al. 1997) also suggested that the electric potential changes both in the precursory rupture nucleation stage (e.g. Ohnaka 1992; Dietrich 1992) and in the subsequent main event were due to piezoelectricity. The amplitude of the precursory signal was 30 times smaller than that of the co-slip signal and this difference could be attributed to the difference of the stress rate as suggested by Eq. 7. The absence or weakening of the signal in the case of non-piezoelectric basalt and wet rocks also supported this view.

Johnston (1997) pointed out two main difficulties with piezoelectricity. Any charges generated in the conductive earth will relax very rapidly with a typical time scale of $2\pi\varepsilon/\sigma \approx 10^{-6}$ s, assuming that the electrical permitivity $\varepsilon$ and electrical conductivity $\sigma$ are respectively $\varepsilon \approx 10^{-10}$ (F/m) and $\sigma \approx 10^{-3}$ (S/m). Any electromagnetic fields propagated from the current source will lose their power very rapidly by Joule dissipation of the conduction current. In order to examine those difficulties, the coseismic electromagnetic amplitude or the waveform due to piezoelectricity, was estimated by evaluating the electromagnetic fields derived from the Green function in the frequency domain (Ogawa and Utada 2000b; Yoshida and Ogawa 2004), or in the time domain (Ogawa and Utada 2000a). Ogawa and Utada (2000a, b) based their estimate of the spatial distribution of the current source due to piezoelectricity on the stress field solution coincident with seismic wave propagation given by Aki and Richards (1980). If a somewhat resistive ($\sigma < 10^{-3}$ S/m) host medium is considered, the estimated electromagnetic field due to a 1 C m electric

dipole (Yoshida and Ogawa 2004), and the first (almost cofracture) electromagnetic signal received before the arrival of the seismic P-wave from an earthquake of magnitude $M_w \geqq 7$ (Ogawa and Utada 2000a), are both marginally detectable at 1–10 km distances from the source, assuming a general noise level of 1–10 mV/km or 0.01–0.1 nT for a period range of 1–10 s (Johnston 1997). Here the 1 C m electric dipole corresponds to a quartzite body of volume $10^8$ $m^3$, subjected to a stress change of 10 MPa. A coseismic stress drop ranges from 1 MPa for inter-plate earthquakes to 10 MPa for intra-plate earthquakes. Yoshida and Ogawa (2004) also argued that detectability of the signals is somewhat enhanced at frequencies higher than $10^6$ Hz, mainly due to the non-relaxation of the piezoelectric polarization in this high frequency range. As a matter of fact, in the laboratory experiment, high frequency electromagnetic emissions could be detected coincident with high frequency acoustic emissions before the main fracture both for dry and wet conditions, whereas low frequency signals died out as reported by Yoshida et al. (1997). But true detectability of the electromagnetic field of piezoelectric origin on the earth's surface may not be very high because of the high conductivity of the earth and the probably small intensity of the stress variation (or that of piezoelectric polarization) in this high frequency range.

*Other Charge Generation Mechanisms*. Besides piezoelectricity, numerous charge generation mechanisms in solid materials have been suggested as potential current sources for electromagnetic signals in association with the crustal activities. These include pressure (stress) stimulated currents with negative activation volume (Varotsos and Alexopoulos 1986; Varotsos et al. 1992), charged dislocations mechanism (Slifkin 1993, 1996; Teisseyer 2001; Stavrakas et al. 2003; Vallianatos et al. 2004), a phase transition associated with large-scale motion of lattice defects (Lazarus 1996), deformation of induced charged flow (Varotsos et al. 2001), a peroxy defects model (Freund 2000, 2002) and rock shearing/triboelectricity (Takeuchi and Nagahama 2002a, b; Roder et al. 2002). All these mechanisms have a physical basis and are respectively supported by related laboratory experiments. However, unless we can explicitly define and determine stress or stress sensitivity as in Eqs. 4, 5 or 7, we cannot easily evaluate the validity of these mechanisms in the real earth.

After the probable charge generation in the seismogenic zone has been estimated in some way, the surface electromagnetic fields due to those charges are calculated. For example, Sarlis et al. (1999) examined the amplification effect due to the existence of the conductivity channel which connects the observation site and the hypocentral region with the aid of the multiple thin sheet code originally developed by Hoversten and Becker (1995) for controlled source methods in electromagnetic prospecting. By putting a 2.26 Am AC current dipole of 0.01 Hz at the hypocentral region, they tried to estimate the amplification effect of a conductive channel of 500 m wide and 200 km in length with a conductance (conductivity times thickness) of 50 S. The host structure was a 2 layered 1-D model with a 50 m surface layer of conductivity $5 \times 10^{-3}$ S/m and a $2.5 \times 10^{-4}$ S/m layer beneath it. As shown in Fig. 5, the signal amplitude is large directly above the source and in a restricted area just above the edge of the conductive channel. In this way, they tried to prove detectablity of their seismic electric signals (SES) emitted from the remote hypocentral region and, at the same time, validate the selectivity rule in their earthquake prediction method (e.g. Varotsos 2005; Varotsos et al. 1993; Kondo et al. 2002). But the existence of such a one to one connection between a sensitive site and its sensitive areas is somewhat unreliable given the rather complicated selectivity rules. It is necessary to prove the existence of such structure by performing extensive MT or controlled source EM surveys.

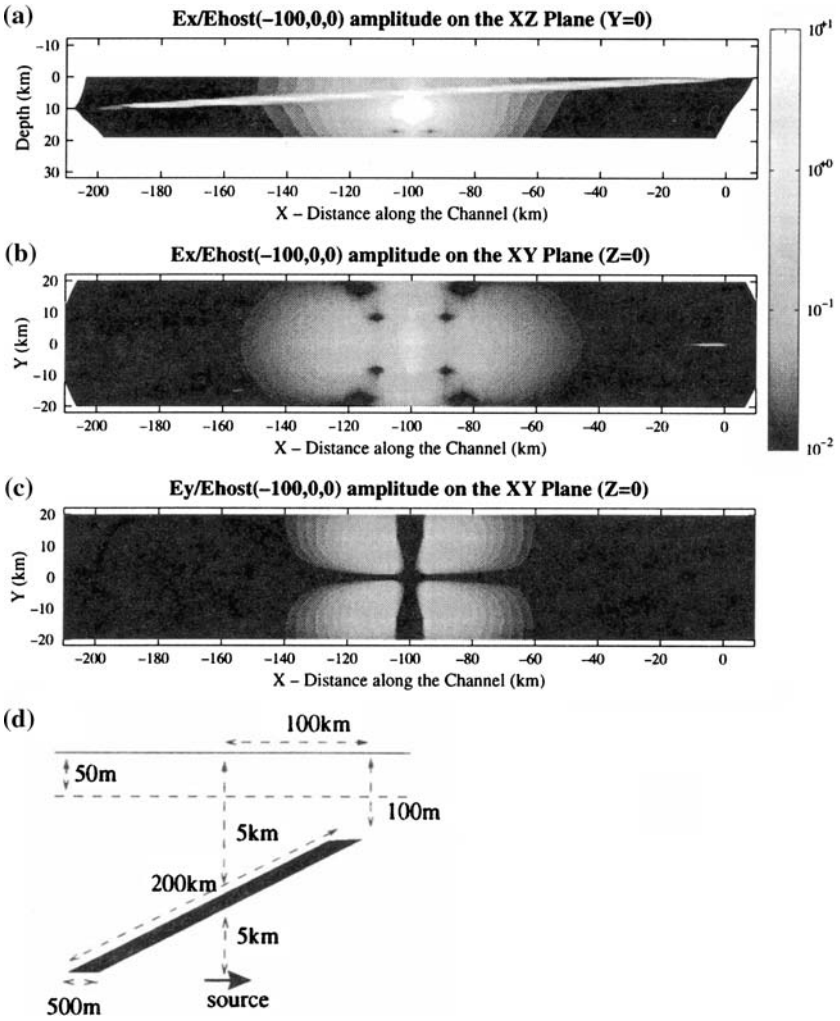


**Fig. 5** Calculated values of the amplitude of horizontal components of the electric field reduced by the value just above the source (at its epicenter on the surface). (**a**) a vertical cross section. (**b**) and (**c**) a plan view. (**d**) a schematic cross section indicating the model (Sarlis et al. 1999)

Both detectability and the selectivity rule have long been matters of controversy together with the origin of their SES (Bernard 1992; Gruszow et al. 1996; Johnston 1997; Uyeshima et al. 1998; Kanda et al. 2000; Pham et al. 1998, 1999, 2001, 2002). As was pointed out by Pham et al. (2002), we must be careful about the existence of abundant charge generators of anthropological origin on the surface. As was also suggested by Chirkov (2004), it will be necessary to determine the spatial distribution of the electromagnetic field and its possible source location, before we can directly connect those signals with crustal activities. We also have to establish the electromagnetic-mechanical coupling equations, such as Eq. 5 or 7, for the respective charge generation mechanisms. Having done that, we can evaluate the stress change that drives charge generation based on these mechanisms. If, coincident with the electromagnetic signals, persuasive geodetic or

seismic evidence also exists to support the determined stress change, then the validity of the existence of the signal will be significantly enhanced. It is, however, important to note that a precise electromagnetic monitoring array (Davis and Johnston 1983; Bakun 1987; Park 1997), located just above the $M_w$ 6.0 Parkfield earthquake, occurring on 28 September, 2004 at a depth of 8.8 km, failed to record any preseismic signals other than coseismic magnetic field steps of between 0.2 and 0.5 nT, and a telluric potential field of 1–2 mV (Langbein et al. 2005; Bakun et al. 2005). This is because the epicentral area directly above the hypocenter is the most sensitive area regardless of the existence of a current channel, as shown by Sarlis et al. (1999).

*Electrokinetic Effects*. Electric polarization occurs on the interface between interstitial water and rock silicates. Under ordinary conditions, negative ions stick to the rock surface leaving an excess of positive ions in the fluids. If fluid motion is driven by a pressure gradient, a flow of the positive ions, i.e. an electric current, is also induced. This is known as the electrokinetic (EK) effect, and has been well investigated for a long time (e.g. Overbeek 1952; Ahmad 1964; Mizutani and Ishido 1976; Ishido and Mizutani 1981). Investigations of the EK effect have been much more activated recently due to its omnipresence and its ability to delineate the sub-surface fluid's motion in association with thermal and mechanical crustal activities. Morphological investigations of the self-potential (SP) anomaly in volcanic areas together with several mechanisms generating SP anomalies were summarized in a recent review paper by Zlotnicki and Nishida (2003).

Since the motion of interstitial fluids is governed by Darcy's Law and its speed is rather slow, problems involving EK effects are normally treated as static. In this case, the macroscopic governing equations describing the relationship between electrical current density $\vec{i}$, fluid volume flux $\vec{j}$, gradients of electrical potential $\phi$ and fluid pressure $P$, are expressed by

$$\vec{i} = -\frac{\sigma_f}{F_1}\nabla\phi + \frac{\varepsilon\varsigma}{F_2\mu}\nabla P \tag{8a}$$

$$\vec{j} = \left(\frac{\varepsilon\varsigma}{F_2\mu}\nabla\phi\right) - \frac{k}{\mu}\nabla P, \tag{8b}$$

where $\sigma_f$, $\varepsilon$, and $\mu$ denote respectively the electrical conductivity, dielectric constant and viscosity of the fluid, and $k$ is the permeability of the fractured rock. $F_1$ is a formation factor representing the ratio $\sigma_f/\sigma_r$ where $\sigma_r$ is the whole rock conductivity including the fluids. If surface conduction is ignored, $F_2$ is equal to $F_1$, and is expressed by the porosity and tortuosity in the capillary model (Ishido and Mizutani 1981). $\zeta$ is the zeta potential, the potential at the slipping plane near the fluid/rock interface. It is a very important parameter characterizing the EK effects. Pride (1994) rigorously derived the time-dependent macroscopic equations which combine Maxwell's equations (Eqs. 1a–d), and the acoustic equations of porous media (Biot 1956).

Revil et al. (1999a, b) derived an analytical equation representing dependence of the zeta potential on mineral/fluid interaction geochemistry (the kinds of mineral lattice and ions in the fluid), pore fluid pH, salinity and temperature. They also derived a similar equation describing the specific surface conductance. The intensity of the zeta potential is shown to increase with increasing temperature and pH (greater than the isoelectric point (IEP), at which the zeta potential is zero (Parks 1965)), and to decrease with increasing salinity. Their equation successfully predicts zeta potentials determined by several laboratory experiments (e.g. Ishido and Mizutani 1981; Tosha et al. 2003; Reppert and Morgan 2003a, b).

The first and second terms of the right-hand side of Eq. 8a represent, respectively, a conduction electric current density due to Ohm's law and a drag electric current density due to the EK effect. The second and first terms of the right-hand side of Eq. 8b, represent, respectively, fluid volume flux due to Darcy's law and fluid volume flux induced by the electric osmotic effect. Since the contribution of the electric osmotic term is smaller by far than the Darcy term, the first term in Eq. 8b is normally neglected, as was also the case in the piezomagnetic and piezoelectric problems. In order to estimate the spatial distribution of SP due to the EK effect, the fluid volume flux is first found and then the electric potential is evaluated by solving an equation such as

$$\vec{i} = -\sigma_r \nabla\phi - \frac{\varepsilon\varsigma}{F_2 k}\vec{j} \tag{9}$$

(e.g. Ishido and Pritchett 1999). Since conservation of charge requires the total current $\vec{i}$ to be divergence-free, Eq. 9 becomes

$$\nabla\cdot(\sigma_r\nabla\phi) = -\left(\nabla\frac{\varepsilon\varsigma}{F_2 k}\right)\cdot\vec{j} - \frac{\varepsilon\varsigma}{F_2 k}\left(\nabla\cdot\vec{j}\right), \tag{10}$$

which takes exactly the same form as an equation used in the DC resistivity method, except that the current source on the right-hand side of Eq. 10 is not of artificial origin. It is clear from Eq. 10, that the electrical current source appears when the fluid flows parallel to the gradient of the material constants (or across a material boundary), or when the fluid flux is not divergence-free. If we have to solve the problem with rather rapid fluid flow, as is sometimes the case in volcanic environments or in fluid motions induced by seismic wave propagation, we also have to solve for the induction effect as we did in the piezoelectric problems.

The zeta potential is negative when pH > IEP and positive when pH < IEP. IEP of $SiO_2$ is about 2. Thus the zeta potential is normally negative and the fluid flux carries positive ions. But volcanic rocks collected around Mt. Takadake in the Aso caldera, SW Japan, show significantly high IEP values up to 8 (Hase et al. 2003). The reason why IEP of some group of rocks is very high has not been fully understood from just the chemical composition of the rocks. Since the polarity of the zeta potential is essential for determining the direction of fluid flow, laboratory experiments to measure the characteristics of the zeta potential are inevitably necessary before an interpretation of the SP anomaly in the field can be made. For example, Hase et al. (2005) found a positive SP anomaly at Mt. Takadake where rocks with positive zeta potential are collected. In the usual case when the zeta-potential is negative, a positive SP anomaly indicates subsurface upward fluid flow due to hydrothermal activity. But Mt. Takadake is rather old and inactive now, and since the zeta-potential is positive, a downward flow turns out to be dominant at that specific peak. The center of present day eruptions is Mt. Nakadake, adjacent to Mt. Takadake, At Mt. Nakadake, there exists an equally positive SP anomaly. But since the zeta potential of the rocks collected around Mt. Nakadake is negative as usual, the positive SP anomaly is interpreted as an indication of upward flow due to hydrothermal activity as seen below.

As is easily recognized from the Eq. 10, determination of the electrical conductivity structure is also very important in interpreting the SP anomaly. In the volcanic area, there often exist W-shape SP anomalies, e.g., at the Miyake-jima volcano, Japan (Sasai et al. 1997), the La Fournaise volcano in Reunion Island, Indian Ocean (Michel and Zlotnicki 1998), Mt. Fuji, Japan (Fig. 6, Aizawa 2004), the Stromboli volcano, Italy (Revil et al. 2004), and the Aso volcano, Japan (Hase et al. 2005). The W-shape SP anomaly is

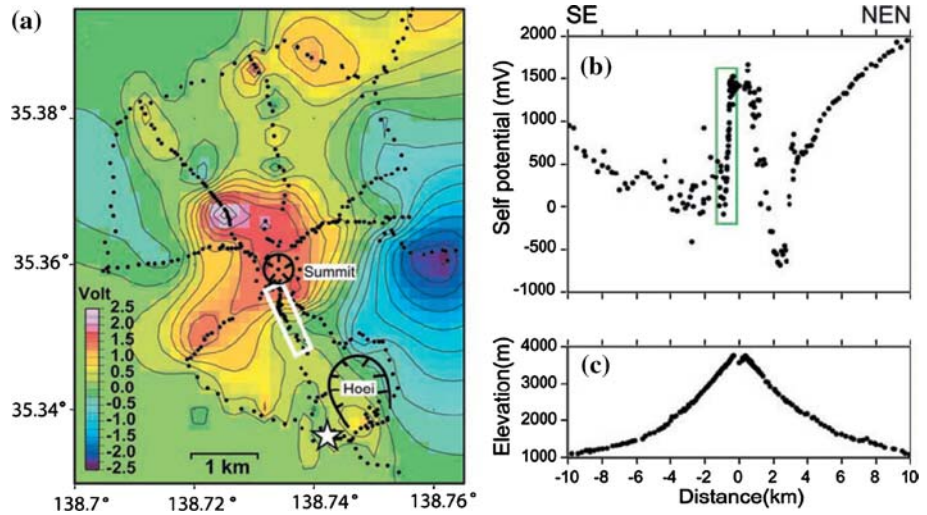


**Fig. 6** Spatial distribution of SP at Mt. Fuji (**a**, **b**) together with its topography (**c**) (Aizawa 2004)

interpreted as a combination of a V-shape anomaly, which is inversely proportional to the altitude of the mountain (topographic effect), with a Λ-shape anomaly whose center is located at the center of the geothermal area. The V-shape anomaly is due to a down-going fluid flow along the slope, and the central Λ-shape anomaly was assumed to be due to hydrothermal convection or vaporization. However, based on numerical computations (Ishido and Pritchett 1999), Ishido (2004) proposed that, in addition to the existence of the hydrothermal convections, an additional area of high electrical conductivity, just beneath the central peak, is necessary to explain the intense central Λ-shape anomaly. A key point in his claim is that the primary cause of the SP pattern is downward liquid motion in the unsaturated thick layer between the surface and the water table in the volcanic body. The EK effect of the downward flow in the unsaturated layer (Guichet et al. 2003) and the underlying saturated layer, results in the shallow and deep regions in the volcanic body having respectively low and high electric potentials. Thus the region of high conductivity beneath the summit acts as a conduit from the region of high potential at depth to the surface. Indeed conductive regions are found just beneath almost all volcano summits (Zlotnicki et al. 2003; Revil et al. 2004; Hase et al. 2005; Aizawa et al. 2005). As an example, Fig. 7 shows such a highly conductive region just beneath Mt. Fuji (Aizawa et al. 2005). Although most authors interpreted the conductive anomaly as an indication of the existence of hydrothermal activity, it could also be due to the presence of clay minerals, for example, after Ishido's (2004) interpretation. Although these different interpretations are still controversial, it is obvious that we need to determine the conductivity structure before interpreting the SP anomaly. Another possible mechanism for generation of the intense central Λ-shape anomaly is the rapid fluid disruption (RFD) effect, recently re-proposed by Johnston et al. (2001) and discussed by Johnston et al. (2002) and Revil (2002). Results suggest that when liquids are vaporized or removed as droplets by gas transport away from hot dike intrusions, charge generation occurs. However, in the case of Mt. Fuji, even though there is no fumarolic activity, the intense central Λ-shape anomaly still exists. Thus, at least in Mt. Fuji area, we can rule out the RFD effect as an explanation of the SP anomaly. In addition to electrical conductivity, temperature is another important parameter

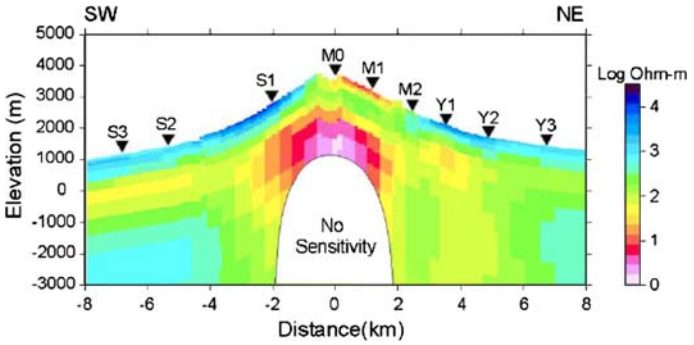


**Fig. 7** Resistivity cross-section at Mt. Fuji determined by wideband MT surveys (Aizawa et al. 2005)

to interpret the SP anomaly. This is because thermal electric coupling can cause the SP anomaly (Corwin and Hoover 1979). For this reason, Lewicki et al. (2003), Revil et al. (2004) and Friedel et al. (2004), for example, measured temperature variation in addition to SP. Lewicki et al. (2003) and Revil et al. (2004) also measured the $CO_2$ gas flux and compared it with the SP and thermal anomalies.

EK effects are also considered to be the main source of electromagnetic signals associated with seismic phenomena. There are several research topics involving seismic phenomena. The first concerns electromagnetic variations due to the vibration of the seismic wave (Russel et al. 1997). This is mainly studied as a potential tool in geophysical exploration (Butler et al. 1996; Mikhailov et al. 1997, 2000; Beamish 1999; Garambois and Dietrich 2001). Based on the macroscopic equations of Pride (1994), Haartsen and Pride (1997) and Garambois and Dietrich (2002) developed full waveform numerical simulation codes of seismo-electromagnetic wave conversions in fluid-saturated stratified porous media. The numerical sensitivity analysis showed that EM waves generated at depth by the passage of seismic waves through an interface are particularly sensitive to contrasts in porosity, permeability, fluid salinity and fluid viscosity. At the surface, the amplitude of electromagnetic waves generated at an interface (at a depth of $\sim$100 m) is 500 times smaller than that of electromagnetic waves contained in the seismic wave reflected at the interface. Thus these phenomena can also be a candidate for the driving mechanism of the coseismic electromagnetic disturbances that are extensively observed (e.g., Skordas et al. 2000; Matsushima et al. 2002; Zlotnicki et al. 2006). Other source mechanisms, such as the electromotive forces induced by vibration of the conductive ground in the presence of the geomagnetic main field, have also been considered (Honkura et al. 2002; Matsushima et al. 2002). The second area of research is monitoring the change in subsurface hydrological parameters and determining in situ EK parameters by injecting water through borehole wells (Wurmstich and Morgan 1994; Murakami et al. 2001; Pinettes et al. 2002; Marquis et al. 2002; Rizzo et al. 2004). The seasonal water level change in artificial lakes or the change of water flux in springs or geysers can also be used for the same purpose (Perrier et al. 1998, 1999; Trique et al. 1999, 2002). The third topic concerns the EK effect as a possible source of seismic precursory electromagnetic phenomena. Mizutani et al. (1976) first proposed that water injection into the dilatant region with low pressure before the main shock—the dilatancy model of Scholz et al. (1973)—can cause electromagnetic disturbances through the EK mechanism. Several model studies (e.g. Fenoglio et al. 1995; Ishido and Prichett 1999; Fujinawa et al. 2002; Simpson and Taflove 2005) have been performed to explain precursory and coseismic electromagnetic

perturbations (Fraser-Smith et al. 1990; Nagao et al. 1996; Fujinawa et al. 2000). In laboratory experiments using a triaxial apparatus, some EK related data have also been collected during rock deformation up to failure (Jouniaux and Pozzi 1995; Yoshida et al. 1998; Lorne et al. 1999; Yoshida 2001). These authors inferred that current sources are generated due to fluid injection into the dilatant region which is formed before the main fracture as a result of the generation of micro cracks. But as the experiment of Yoshida (2001) clearly indicated, the intensity of the electric signal together with the dilatancy grows toward the onset of the main fracture, with the most significant signal being obtained at the time of the main fracture itself, as was the case with the piezoelectric experiments (Yoshida et al. 1997). Although some field results show such features (e.g. Fraser-Smith et al. 1990; Hattori et al. 2004), isolated signals often reported well before earthquake onset are not concordant with these laboratory experimental results. Furthermore, it is not easy to monitor fluid motion at depth unless some special condition is considered. For example, in order to explain the amplitude of the SP variation observed by Nagao et al. (1996), Ishido and Prichett (1999) needed vaporization in the dilatancy area and a conductive fault zone connecting the dilatancy area and the near surface. Even in the above mentioned fluid injection experiments using boreholes, a clear signal could be detected on the surface when a metal casing was inserted in the borehole (e.g. Murakami et al. 2001; Marquis et al. 2002). Otherwise, as is argued by Pinettes et al. (2002), it is not easy to detect streaming potentials generated at depth, because the injection induced flow generates dipolar current sources at depth.

### 2.2.3 *Electrical Conductivity*

Electrical conductivity is especially sensitive to the existence of interstitial fluids, their connectivity and temperature. The electrical conductivity of dry rocks in the temperature range in the crustal condition is very low in comparison with the high conductivity of interstitial fluids, clay minerals or carbon films in the same low temperature range (e.g., Kariya and Shankland 1983; Nesbitt 1993; Frost et al. 1989). Almost all the electrical conductivity values determined from the field surveys range between those of resistive dry rocks and interstitial highly conductive phases, and the connection rule of the highly conductive phase is important in determining whole rock electrical conductivities (e.g. Glover et al. 2000b; Bahr 2000; Bahr et al. 2002). Thus electrical conductivity is likely to be very sensitive to the temporal variation of the connection rule due to strain changes (Glover et al. 2000a; Hautot and Tarits 2002). Graphitization during fracture (Roberts et al. 1999) is also a possible mechanism for changes in electrical conductivity.

Laboratory experiments have shown that the stress sensitivity of electrical conductivity in saturated rocks is 0.025%/bar ($2.5 \times 10^{-9}$/Pa) (Brace and Orange 1968a, b), which is 75 in strain sensitivity ($\Delta\sigma/\sigma/\Delta\ell/\ell$) if a rigidity of $3 \times 10^{10}$ Pa is assumed. For porous rocks such as tuffs, strain sensitivities are much enhanced, ranging from several hundreds (Yamazaki 1965, 1966) to as large as $10^4$ (Morrow and Brace 1981) in partially saturated cases. Since tidal strain amplitude is in the order of $10^{-7}$, and the inter-seismic strain accumulation rate in Japan, revealed by GPS measurement, is of order $10^{-7}$/year (e.g. Sagiya et al. 2000), the corresponding conductivity changes are, respectively, $10^{-3}$ (0.1%) and $10^{-3}$/year (0.1%/year) at most. Even considering localized acceleration of the strain accumulation rate before the earthquake, realistic conductivity changes are likely to be a few percent at most. Park and Fitterman (1990), Park (2002) and Hanekop and Simpson (2006) have all argued that it is difficult to detect such a small-localized conductivity

change by using the natural source MT method, unless observations are made in close proximity to the seismogenic zone with an accurate measurement technique.

In contrast, electrical conductivity changes reported in field experiments spanning scales of kilometers are enigmatic because the strain amplification factors should be much larger than those obtained from the laboratory experiments. Changes in telluric responses of 0.2% per year beginning in 1986 are attributed to a 50% decrease in the resistivity along deep portions of the San Andreas fault (Madden et al. 1993). Results from China show a gradual increase in the electrical conductivity of the shallow crust at multiple sites spanning an area of square kilometers (Zhao and Qian 1994; Chu et al. 1996). These changes began 4 years prior to the 1976 Tangshan earthquake, peaked at an approximate 4% decrease in apparent resistivity, and then recovered in the 4 years after the event.

Conductivity changes monitored by the DC resistivity method in a vault at Aburatsubo, central Japan, spanning a scale of meters (Yamazaki 1967) were also enigmatic. Although the daily variation of order $10^{-4}$ can be explained by tidal strain, the annual variation of order $10^{-2}$, together with coseismic steps of order $10^{-4}$, cannot be explained by the strain effect on the electrical conductivity. Utada et al. (1998) proposed that these last two temporal variations can be explained as electrical conductivity variations due to, respectively, a temporal change of temperature ($10^{-4}$/0.01°C), and a temperature change resulting from a mixing of fluids on the arrival of the S-wave. In this model, the vertical gradient of temperature just around the vault is a key parameter and the seasonal variation of the temperature gradient was confirmed by subsequent thermal measurements (Perrier et al. 2004). Although a number of preseismic conductivity changes were also reported by Rikitake and Yamazaki (1976), Utada et al. (1998) recognized no clear precursory change when irregular changes due to bad weather or instrumental instability were properly eliminated.

In comparison with seismic phenomena, the temporal variation of electrical conductivity in volcanic and geothermal areas is much larger because of the large variation in temperature and water content (or vaporization) associated with magma intrusion. Magma or melts are themselves also several orders of magnitude more conductive than igneous rocks (e.g. Tyburczy and Waff 1983). The presence of an interstitial aquifer also controls a variety of volcanic activities through the interaction of water and hot materials (e.g. Kagiyama et al. 1999). Therefore, it is very important to monitor the temporal variation of the electrical conductivity structure in volcanic environments. Monitoring is also desirable in interpreting the temporal variation of the SP anomaly, as was discussed before. The technical difficulty of maintaining long-term operations involving measurements of high accuracy in the difficult environmental conditions of volcanic areas, however, has prevented most researchers from detecting the time evolution of the conductivity structure in volcanic regions. Exceptions are the conductivity monitoring on Oshima volcanic island, Japan (Fig. 8; Yukutake et al. 1990) from 1975 to the present, and on Miyake volcanic island, Japan (Zlotnicki et al. 2003) from 1999 until the formation of the large sink-hole in the 2000 eruption. In both cases, the DC resistivity method was applied in the vicinity of the summit and the temporal variation of the apparent resistivities measured on several sets of transmitter–receiver combinations were continuously monitored. Based on the records of the 1986–1987 activity on the Oshima volcano, Utada (2003) proposed a model of the temporal evolution of the magma intrusion before the first eruption on November 15, 1986, as shown in Fig. 9. Zlotnicki et al. (2003) found a drastic apparent resistivity change on July 3, 2000, only 5 days before the generation of the sinkhole. The apparent resistivity decreased to 20% of its initial value in 1999 on the 600 m line while it had reached more than three times its original value on the 1,400 m line. This suggests the possibility that the

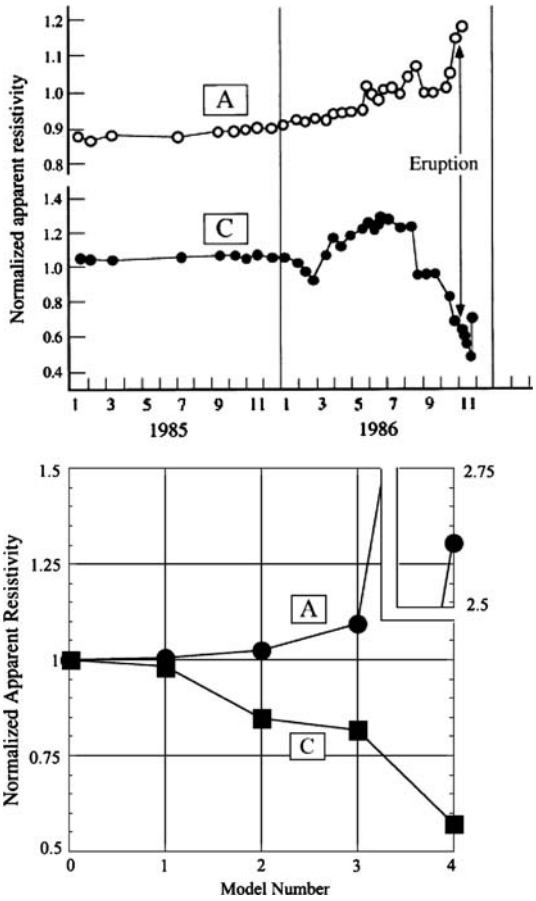


**Fig. 8** Observed temporal changes in the apparent resistivities for receivers 'A' and 'C' in 1985 and 1986 (Yukutake et al. 1990) are shown in the upper panel, where apparent resistivity values are normalized by corresponding values at the first measurement. The vertical line with arrowheads indicates the onset of the summit eruption. Synthetic apparent resistivities based on the models in Fig. 9 are shown in the lower panel (Utada 2003)

area of the future sinkhole turned resistive before the onset of its generation. The variation of total magnetic intensity also indicated that demagnetization occurred from deeper to shallower regions, and is interpreted as the generation of a magnetically void area due to the magnetized body being crushed (Sasai et al. 2002).

## 3 Network-MT Observations

### 3.1 Introduction of the Network-MT Observation Method

Due to recent remarkable progress in determining MT response functions, which is both due to improvements to instrumentation and to the robust processing method (e.g. Egbert and Booker 1986; Chave et al. 1987), all of the elements of the impedance tensor can be determined with sufficient accuracy such that full-tensor interpretation has become feasible. Considerable efforts have been aimed at decomposing observed MT responses into the component caused by local three-dimensional (3-D) galvanic distortion and that induced by regional one- or two-dimensional (1-D or 2-D) structures (Bahr 1988; Groom and Bailey 1989; Groom and Bahr 1992; Chave and Smith 1994). Phase tensor analysis

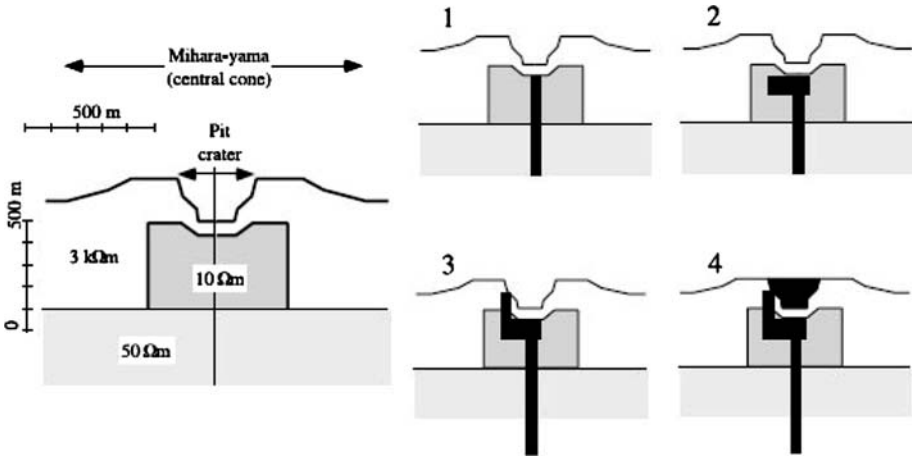


**Fig. 9** Cross-section of the subsurface resistivity structure for numerical forward modeling. As a background structure, a two-layered model was assumed with a localized anomalously conducting zone beneath the pit crater (model 0 shown in left-hand side). The ascent of the magma and the formation of lava lake were simulated by adding conducting (0.5 Ωm) bodies in Models 1 to 4 (Utada 2003)

(Caldwell et al. 2004) and tensor invariants analysis (Weaver et al. 2000; Martí et al. 2005) can discriminate dimensionality of regional structure. Together with the progress of 2-D inversion algorithms combined with static shift correction (e.g. deGroot-Hedlin 1991; Ogawa and Uchida 1996), MT tensor decomposition coupled with this hybrid 2-D interpretation is the currently accepted procedure for interpreting MT responses (see the review paper by Ogawa 2002). Furthermore, with developments of 3-D forward/inversion codes and faster computer facilities, 3-D modeling has become more common (see the review paper by Avdeev 2005).

Even with this progress, the problem of the static shift correction still remains in determining deep large-scale structures. As far as we deploy conventional MT measurements with short electric dipoles ($\sim$100 m electrode spacing), the respective voltage difference records are inevitably contaminated by galvanic effects due to small-scale near-surface lateral heterogeneities of electrical conductivity. This inherent short wavelength spatial variation of the electric field, however, cannot be represented in observations unless we sample the electric field with sufficiently high spatial density. Therefore, static shift is often corrected in the inversion process based on some statistical assumption. Because of the non-uniqueness of its determination, however, especially when the spatial sampling density or the quality of the MT responses are not sufficient, we sometimes encounter cases where models exist with different sets of static corrections, but with almost comparable RMS values. Structure models with different static shift corrections possess different length scales together with different spatial contrasts in electrical conductivity. One way to alleviate this difficulty is to estimate the static shift correction levels by referring to the magnetic transfer functions, since rotation of the static shift free impedances should be equivalent with the static shift free magnetic transfer functions (Utada and Munekane 2000). Another approach is to obtain spatially integrated electrical potential differences either by using long dipoles or by deploying an array of dipoles whose scale lengths fit those of the target structure (Jones 1988; Torres-Verdin and Bostick 1992a, b; Singer 1992).

Figure 10 demonstrates the effect of spatial filtering in the TM mode of 2-D problem. As a test model, a simple 1-D 2 layer host structure (0.002 S/m down to 400 km and 1 S/m

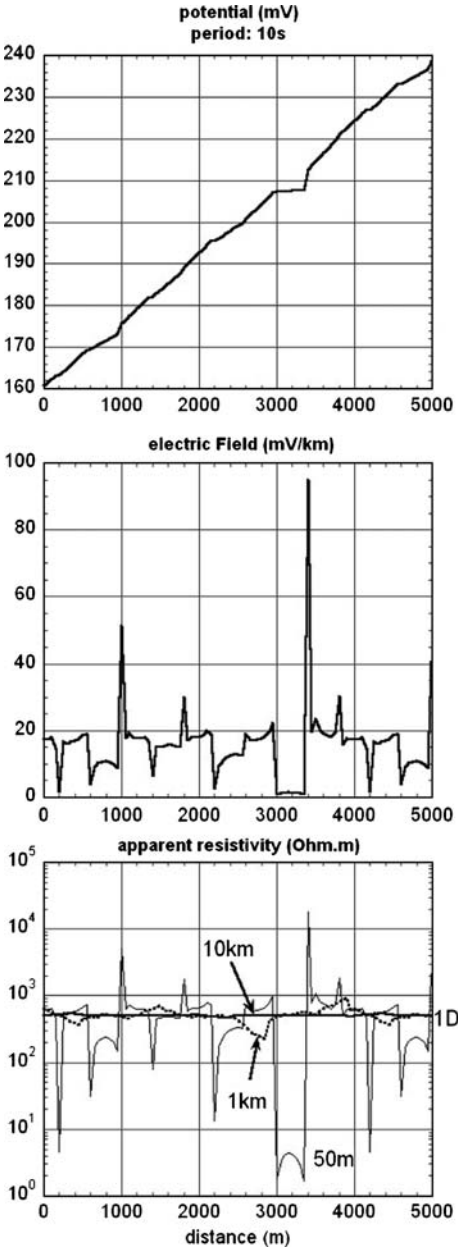


**Fig. 10** A 2-D TM-mode model study to demonstrate effect of long-baseline electric field measurements. As a test model, a simple 1-D 2 layer host model is assumed and randomly changed conductivity values are assigned in the surface top layer with 5 m thickness. Spatial distribution of electric potential (top), electric field (center), and apparent resistivity from measurements with various dipole lengths (bottom) are shown

beneath 400 km) is assumed, and 10 conductivity values between 0.0002 S/m and 1 S/m are randomly assigned to blocks 400 m wide and 5 m thick in the top surface layer. EM fields with plane wave excitation are first computed with the aid of the FEM 2-D forward modeling scheme of Wannamaker et al. (1986) and plotted in the middle of Fig. 10. Then voltage differences between a reference point and various locations are estimated by integrating the relevant electric fields. From the voltage difference (or electric potential) profile shown in the top of Fig. 10, voltage differences for 50 m, 1 km and 10 km

electrode spacings, average electric fields, and finally apparent resistivities for respective dipole lengths are calculated and plotted in the bottom of Fig. 10. Due to charges on the vertical boundaries in the top layer, the electric fields, and therefore the impedances, are significantly scattered, whereas the overall linear trend of the electric potential is little affected by the charges. Then, as the baseline lengths for the electric field measurements increase, the effects of the boundary charges are reduced, and the static shift problem can be alleviated. It is, however, noteworthy that even the Network-MT impedances contain a static effect. The quasi-static Maxwell equations yield exactly the same solution with a scale change given by the relationship $\sigma \times \mu \times L^2 / T = \text{const}$, where $\sigma$, $\mu$, L and T are scales of electrical conductivity, magnetic permeability, length and period respectively. Thus, for example, a scaling factor of 1/200 for conductivities and 200 for periods and lengths gives the same solution. This means that static shifts prominent with 50 m dipoles in Fig. 10 are also prominent with 10 km dipoles under this scale change. In this sense, we cannot escape from static shift effects. An important point is that surface blocks with a typical horizontal scale length of 400 m cannot be incorporated especially in 3-D regional modeling, whereas surface blocks with 80 km scale length can be.

### 3.2 Regional Scale Network-MT observation

Thus, to determine the 3-D structure of deep electrical conductivity on a nationwide scale, e.g. over an area several hundreds of $km^2$, the electric field had better be measured with a typical dipole length of 10 km or more. In order to estimate the spatial variation of the structure on this scale, all the electrodes are ideally mutually connected by the observation network. Recently, referring to the pioneering works in employing telephone lines for electric dipoles (e.g., Rooney 1949; Egbert and Booker 1992; Egbert et al. 1992; Madden 1983; Madden et al. 1993; Mori 1985, 1987; Tournerie and Chouteau 1998), Uyeshima et al. (2001) have developed an observation technique named "Network- MT method". In this method, the telephone line network is fully used to determine the horizontal distribution of voltage differences with long electrode spacings. Figure 11 illustrates a typical (and ideal) configuration of the Network-MT experiment. The dipoles in this illustration are telephone lines connected to electrodes, which are either earths installed for telecommunication facilities by the telephone company, or electrodes purpose built for the experiment. Dipole lengths range from ten to several tens of kilometers. As a reference magnetic field, magnetic records obtained by three-component magnetometers at

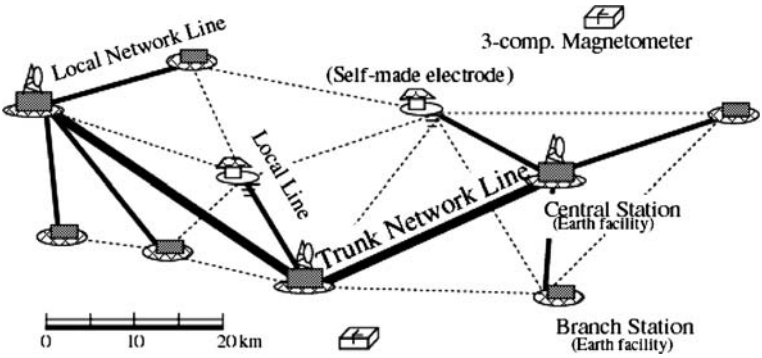


**Fig. 11** A sketch of Network-MT observation

geomagnetic observatories or at purpose-built stations are used. The spatial distribution of the electric fields in the target region is obtained by combining two types of observation. One uses local telephone lines directly. The other links local telephone line observations using network trunk connection lines. Since the local telephone lines, as well as the network trunk connection lines, are connected to the central telephone station within a particular telephone toll area, data loggers are installed at the central telephone station. In an actual field survey, voltage measurements are performed at several toll areas at once for a few months and then moved to other toll areas because of the restricted number of instruments. Another way to measure the spatial distribution of long baseline voltage differences is to measure the Geomagnetically Induced Currents (GIC) in power line networks or pipeline networks (see, for example, review papers by Viljanen and Pirhola 1994 and Campbell 1986). If we deploy long dipoles, the S/N ratio of the electrical records will be enhanced. This enhancement will enable us to extend the experiment both in the space and frequency domain (especially toward the lower frequency range).

After the telluric voltage difference records are obtained, response functions between each voltage difference and 2-component horizontal magnetic fields are estimated. The period range is from several seconds to $10^5$ or $10^6$ s. Assuming that the response functions $Y_x(\omega)$ and $Y_y(\omega)$ are expressed as

$$V(\omega) = Y_x(\omega)H_x^r(\omega) + Y_y(\omega)H_y^r(\omega), \tag{11}$$

where for an angular frequency $\omega$, $V(\omega)$, $H_x^r(\omega)$ and $H_y^r(\omega)$ are respectively the voltage difference along a dipole and two component horizontal magnetic fields at a reference site, and $Y_x(\omega)$ and $Y_y(\omega)$ are the voltage differences occurring when a unit magnetic variation occurs respectively in the $x$(NS)-direction and the $y$(EW)-direction at the reference site. If all the electrode points are connected by the observation network as shown in Fig. 11, the virtual voltage difference between any pairs of electrodes can be estimated by a linear combination of the response functions for real (or measured) dipoles. In this way, after selecting three electrode points in the observation area, the voltage differences along two sides of the triangle formed by the selected electrode points can be estimated, and then, the average 2-component electric fields in the triangle, when a unit magnetic variation occurs in the $x$- or $y$-direction at the reference site, can be estimated by linear combination of the response functions $Y_x(\omega)$ or $Y_y(\omega)$, respectively. Thus the average impedance tensor for the triangle can be estimated. In Fig. 12, the spatial distributions of the vectors (Re(Zxx), Re(Zyx)), (Im(Zxx), Im(Zyx)), (Re(Zxy), Re(Zyy)) and (Im(Zxy), Im(Zyy)) in the central and eastern parts of Hokkaido, Japan, are plotted (Uyeshima et al. 2001), where Zij is the ij-th element of the impedance tensor estimated by the above procedure. The period is 3840 s. The vector (Re(Zxx), Re(Zyx)) can be recognized as the electric field in the time domain due to a unit sinusoidal magnetic field variation in the N–S direction when the magnetic field at the reference station (Memambetsu geomagnetic observatory of the Japan Meteorological Agency) points to the north with maximum amplitude. The vector (Im(Zxx), Im(Zyx)) can be recognized as the electric field in the time domain due to a unit sinusoidal magnetic field variation in the N–S direction when its direction is changing from southwards to northwards, with its amplitude being zero. Likewise, the respective vectors (Re(Zxy), Re(Zyy)) and (Im(Zxy), Im(Zyy)) represent the electric fields due to a unit E–W magnetic field variation when the magnetic field points to the east with maximum amplitude, and when its direction is changing from westwards to eastwards with its amplitude being zero. Given a 1-D subsurface structure, and an impedance phase between 0 and $\pi/2$, all the electric field vectors of (Re(Zxx), Re(Zyx)) and (Im(Zxx), Im(Zyx))

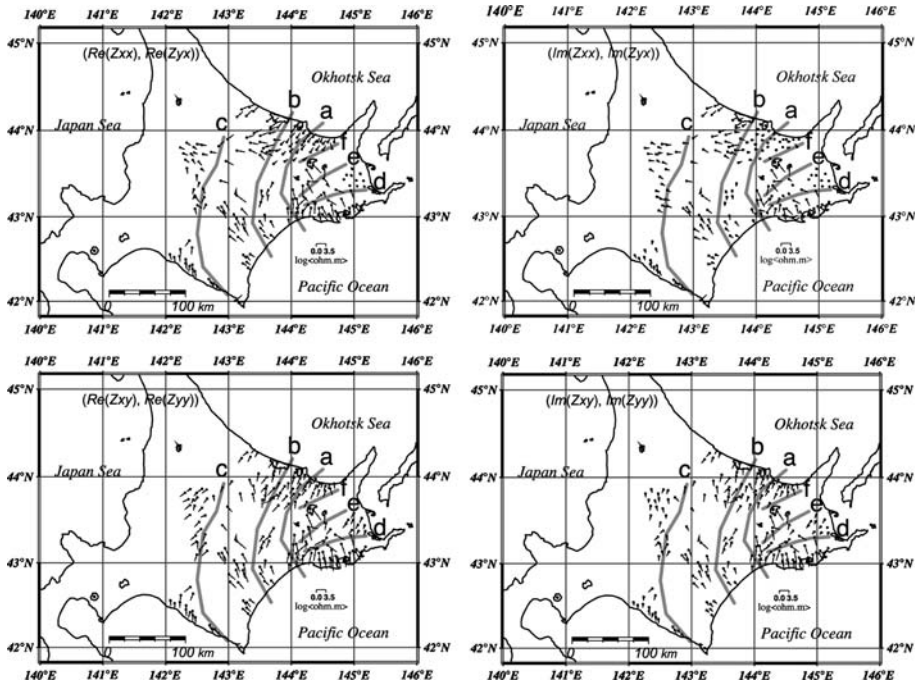


**Fig. 12** Spatial distribution of impedance tensors for a period of 3840 s. Vectors (Re(Zxx), Re(Zyx)), (Im(Zxx), Im(Zyx)), (Re(Zxy), Re(Zyy)) and (Im(Zxy), Im(Zyy)) are shown, respectively. The vectors are plotted in lines with arrow heads indicating the azimuth of the vector. The length of the line is proportional to the logarithm of the vector's absolute value in the unit of apparent resistivity. No vectors are indicated if the apparent resistivity value is less than 1 Ωm. Geoelectrical structure boundaries interpreted from the maps are also shown by thick shaded lines

would point westwards, and those of (Re(Zxy), Re(Zyy)) and (Im(Zxy), Im(Zyy)) would point northwards. In the present target region, however, the electric field vectors are not uniformly distributed as mentioned above, but are significantly distorted. Note that each vector in Fig. 12 represents the averaged impedance tensor for triangular sections of typically 10 km length scale. Then it is also noteworthy that the electric field vectors, which were derived directly from the respective elements of the impedance tensors, point in similar directions for adjacent sections, so some regional trend can be detected. This result shows that the Network-MT responses are relatively free from the effects of small-scale near-surface structures. The figures also show geoelectrical structure boundaries (thick shaded lines), which were obtained by interpreting the spatial distributions of the intensity and azimuth of the vectors. These boundaries correspond either to major tectonic lines (a, b and c) or to boundaries of a geological unit (d, e and f) in the region.

In order to obtain regional 2-D or 3-D structures from the Network-MT data, several methods were developed. One way is to first compose averaged impedance tensors for triangles formed by three electrode points, as mentioned above, and then, conventional inversion schemes are applied to those impedance tensors (Yamaguchi et al. 1999; Shiozaki et al. 1999; Satoh et al. 2001). In Satoh et al. (2001), Network-MT and conventional MT impedances were jointly inverted by a 2-D inversion code (Ogawa and Uchida 1996) with the static shift correction determined in the inversion. Although the static shift parameters are set to be freely determined in the inversion, the resultant static shifts for

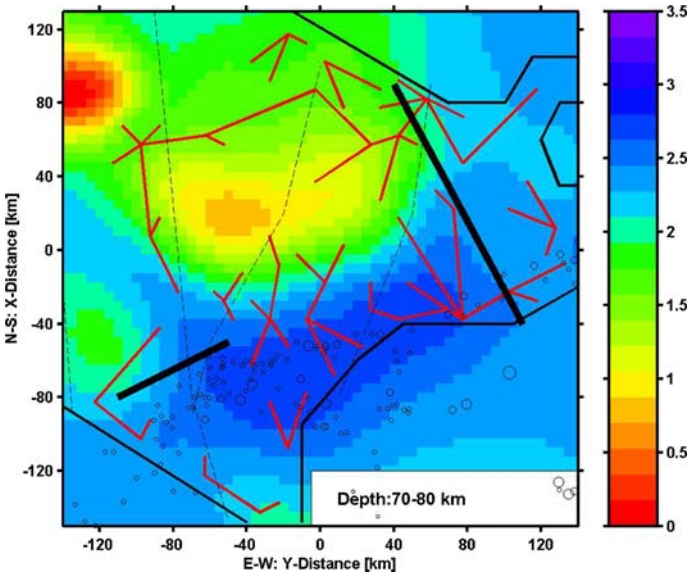


**Fig. 13** Electrical conductivity distribution at depths of 70–80 km beneath eastern part of Hokkaido, SW end of Kuril arc. Red lines are dipoles used in the 3-D inversion (Uyeshima et al., in preparation)

Network-MT data turn out to be almost unity. This also suggests that static shift in Network-MT data can be expressed in the regional model. In Uyeshima et al. (2001, 2002), the response functions between the respective voltage difference and magnetic field are directly reproduced in the 2-D or 3-D forward calculations. This method has been adopted in a subsequent 3-D inversion scheme by Siripunvaraporn et al. (2004), which is based on 2-D and 3-D data space Occam inversions designed for inverting conventional MT datasets (Siripunvaraporn and Egbert 2000; Siripunvaraporn et al. 2005). Figure 13 shows a resistivity structure at depths of 70–80 km beneath the eastern part of Hokkaido, at the SW end of the Kuril arc, which is determined from a full 3-D inversion code (Uyeshima et al., in preparation). The seismically active part of the subducting Pacific slab is imaged by a resistive belt, and the conductive back arc wedge mantle is imaged in the model.

### 3.3 Local Scale Network-MT observation

The concept of the original large-scale Network-MT observation is also applicable to local studies, typically on a scale of 10 km$^2$. In this case, electrodes are distributed with, on average, several hundred meters to 1 km spacings in the target area. Examples of such studies are telluric monitoring networks in Parkfield, USA (e.g. Park and Fitterman 1990), in Miyake Island, Japan (e.g. Sasai et al. 1997), and in the French Alps (e.g. Perrier et al. 1998). Although the first two experiments also use the telephone lines to connect electrodes, in the French Alps the observation network was constructed by the researchers' own efforts. In relation to the large-scale Network-MT survey described above, the triangular sections of typically 10 km size where the regional impedance tensor (e.g. as shown in Fig. 12) is estimated, are further subdivided by sets of electrodes, (e.g., 5, 9 and 14 electrode points respectively for the Parkfield, Miyake and French Alps experiments). All the voltage difference recordings on this scale may contain galvanic effects from near

surface heterogeneities on a local scale, in addition to information on a regional scale as shown in Fig. 12. In order to obtain the regional scale impedance in the French Alps experiment, a single averaged impedance tensor was estimated by using all the response functions, as expressed by Eq. 11, for all the dipoles (Tarits et al. 2004). Furthermore, they determined a 1-D impedance free from static effects with the aid of GDS responses over a longer period range. Once such a regional 1-D impedance has been estimated, the galvanic distortion parameters for the respective dipoles can be estimated. Since the galvanic parameters are determined by the locally uniform induced current and the near surface lateral variation of the electrical conductivity, the near surface electrical conductivity structure can be estimated in some way with the aid of a 3-D DC code (e.g. Spitzer 1995). In this way, Hautot (2005) determines a shallow 3-D electrical conductivity structure, also referring to an electrical conductivity model previously obtained from 2-D and 3-D analyses of the VLF and AMT data (Hautot et al. 2002). Thus, in addition to monitoring the temporal variation of the SP field in a target area, the temporal variation of the galvanic parameters can be used to monitor the temporal variation of the shallow electrical conductivity structure, as discussed in the next section.

Recently, since trunk and local network lines, as shown in Fig. 11, have been almost completely replaced by optical fiber cables, it has been necessary to make measurements using only local lines. Therefore, when we want to determine a large-scale structure, an assemblage of local observations has to be made, and voltage recording instruments are installed both at central telephone stations and branch repeater stations. A Network-MT survey in the NE part of China by Ichiki et al. (2001) is one example of this type, where four long baseline dipoles of length 20–40 km were used in a target area 200 km square. In order to determine the deep structure, they first estimated mutually perpendicular impedances from Eq. 11 and rotation of the magnetic field coordinates. After static shift correction with the aid of the GDS responses, and by using the $\rho+$ inversion scheme (Parker and Booker 1996), they determined four 1-D structures as shown in Fig. 14.

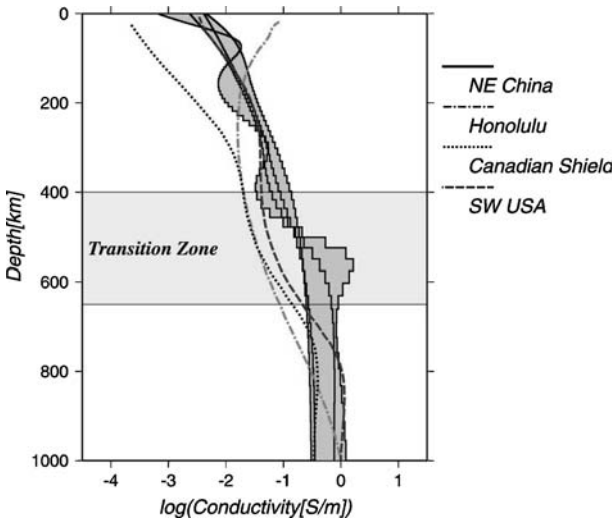


**Fig. 14** Comparison of 1-D conductivity profiles in NE China (solid line with shaded area) with those at Honolulu (chain line), Canadian Shield (dotted line) and SW USA (broken line) (Neal et al. 2000). The mantle transition zone is shown by thinly hatched area (Ichiki et al. 2001)

The 1-D structures obtained by Neal et al. (2000) are also shown in the figure. NE China is located in the area where seismic tomography has revealed a stagnant Pacific Plate with high seismic velocity on the boundary between the upper mantle and the lower mantle (Fukao et al. 2001). The size of the stagnant slab in this region is several thousands of kilometers. Probably due to a fluid supply from the stagnant slab, the electrical conductivity in and above the transition zone is higher than the conductivities determined by Neal et al. (2000), although the temperature is low due to the existence of the slab (Ichiki et al. 2006). Tarits et al. (2004) also determined a deep 1-D structure by inverting the average 1-D impedance, as was described in the previous paragraph. A similar relatively conductive feature is obtained above the stagnant slab beneath the French Alps.

### 3.4 Network-MT Observation as a Tool to monitor Crustal Activities

Since Network-MT observations record continuous telluric voltage differences together with the magnetic field, the datasets can also be used to monitor electromagnetic phenomena related to crustal activities. Network-MT observations in Japan by Kinoshita et al. (1989) and Uyeshima et al. (1989) were initially aimed at detecting seismic electric signals (Varotsos and Alexopoulos 1984a, b). Several coseismic signals were obtained at multiple electrode points, so that its spatial field pattern could be drawn, as reported by Kinoshita et al. (1989), Sumitomo et al. (1997) and Nagao et al. (2000). Possible preseismic signals reported by Uyeshima et al. (1989), Nagao et al. (1996) and Uyeda et al. (2000, 2002), however, are enigmatic, because they were almost always detected in the vicinity of a single electrode point. One exception was that Uyeda et al. (2000) simultaneously acquired anomalous signals of similar boxcar shape at three widely separated independent stations, approximately 100 km apart, in central Japan, 11 days before onset of a small swarm activity which occurred almost at the center of these three sites. However, they could not trace the origin of the signals.

Analysis of datasets from the long baseline array monitoring the telluric field near two artificial lakes in the French Alps, clearly shows that annual SP variations were detected at electrodes near the bank of the artificial lakes. The water level of both lakes was high in the summer and low in the winter due to the seasonal variation of the electric power supply. These SP variations were interpreted to be caused by electrokinetic effects associated with alterations to the pattern of underground fluid flow induced by the change of water level in the lakes (Perrier et al. 1998; Trique et al. 1999, 2002). In addition, Hautot (2005) found an annual variation in the galvanic parameters, which are separate from the response functions expressed by Eq. 11. Based on the DC 3-D model mentioned in the previous subsection, it was inferred that a resistivity variation of 20% in the bedrock could account for the observed annual variation in the galvanic parameters. This resistivity variation was ascribed to a change of strain resulting from the change of lake water loading as the water level changed. But even if the highest amplification factor of $10^4$ (Morrow and Brace 1981) is assumed, a strain variation of order $10^{-5}$ seems necessary to explain the resistivity variation, whereas the annual strain variation is estimated to be of order $10^{-7}$. It has been argued that a further large increase in sensitivity can be expected when the saturation of the rock is near the percolation threshold (Hautot and Tarits 2002). However, the resistivity variation due to temperature change may be another candidate, as mentioned in the previous monitoring section. A similar attempt was made by Park (1991, 1997, 2002) in Parkfield, California with kilometer scale telluric arrays. After determination of the conductivity structure by an active DC resistivity survey at Parkfield, sensitivities of the

telluric array to various model blocks were calculated (Park and Fitterman 1990). Since the telluric array reportedly could not detect any significant preseismic fluctuation before the $M_w$ 6.0 Parkfield earthquake on 28 September 2004 at a depth of 8.8 km (Langbein et al. 2005; Bakun et al. 2005), resistivity changes before the earthquake should be less than those detectable limits.

Network-MT observations have also been performed in volcanic areas such as the Oshima, Unzen, Aso and Miyake-Jima volcanoes in Japan. In a series of volcanic activities during the 2000 eruption on Miyake-Jima volcanic island, several kinds of electric signals were acquired by the Network-MT observation, which are probably associated with electrokinetic effects (Sasai et al. 2001a, b, 2002). Coincident with the generation of the large sinkhole on July 8, 2000 and during the subsequent tilt step events—very long period ($\sim$40 s) seismic activities which represent inflations (Ukawa et al. 2000; Kumagai et al. 2001)—until August 18, 2000, the variation of the electric field was observed to be very similar to the velocity waveform of the seismograms, with almost the same field pattern over the whole island. Since the SP variation near the summit was negative, these signals were interpreted as a result of ground water flow away from the pressure source at a depth of about 3 km. A similar SP variation coincident with long period seismic activity was observed at the Merapi volcano (Byrdina et al. 2003). Subsequently, a significant enhancement of SP at one electrode near the summit was observed during an intense eruption on August 18. This indicated that the eruption had caused some drastic changes in the hydrothermal system.

## 4 Conclusion

Recent progress in the development of electromagnetic methods aimed at monitoring volcanic and seismic activities has been reviewed with reference to the various driving mechanisms that can generate electromagnetic sources at depths. Intensive laboratory and theoretical research is advancing our understanding of the basic relationships between the intensity of the respective electromagnetic sources and changes in the mechanical, chemical and thermal states. Also with the progress being made in electromagnetic simulation techniques, it has become possible to evaluate in situ sensitivity. Based on this progress and with extensive developments having been made in techniques of measurement and data processing, many field experiments have been conducted to elucidate temperature variation, stress or strain change, water content variation and its movements at depth related to crustal activities. The usefulness of electromagnetic methods, however, seems to be more established in volcanic research than in seismic research. This is probably due to the difference in recurrence time of volcanic and seismic activities, as well as with their intensity and variation speed, and difference in depths of sources. Observations in the proximity of the activity can be realized in volcanic research but is normally difficult in seismic research, and further refinements in observation and data processing techniques will be necessary in order to capture the much smaller seismic signals. At the same time, we must be more careful about the sources near the surface which have no causal relationship with crustal activities.

A Network-MT observation technique has been developed to determine a regional scale deep electrical conductivity structure over a region several hundreds of $km^2$, in which a telephone line network is fully utilized to measure telluric potential differences with long electrode separations. Due to the averaging effect, the response functions in the method are relatively free from static shift caused by complicated near-surface small-scale lateral

heterogeneities. The method was first utilized to determine regional scale 2-D structures with the aid of conventional 2-D inversion codes. Owing to recent progress in inversion schemes, 3-D regional structures can now be determined. Several field experiments have been performed to obtain from 1-D to 3-D deep and regional electrical conductivity structures in target areas where slab subduction or its stagnation occurs. All the structures have some relationship with existing slabs and they will be useful to elucidate mechanisms of large-scale tectonic activity related to plate subduction. The technique can be applied also to monitor regional or local scale temporal variation of the telluric fields together with the electrical conductivity structures related to the crustal activities. In the French Alps, annual variations of voltage difference and conductivity were interpreted in terms of respectively the electrokinetic phenomenon and strain change due to annual variation of the lake water level. The method was also used to monitor variation of the voltage differences and the electrical conductivity structure in the preparation stage and onset of the earthquakes and volcanic eruptions.

**Acknowledgements** First of all, I acknowledge the IAGA working group 1.2 for providing me an opportunity to present this review paper at the 18th Electromagnetic Induction Workshop at El Vendrell, Spain. I also want to express my sincere thanks to all the contributors to this review. Critical reviews from A. Martí and an anonymous reviewer, as well as kind help from J. Weaver (a guest editor of this issue), have significantly enhanced the clarity and quality of this paper.

## References

Abdullabekov KN, Berdaliyev YE, Pushkov AN et al (1979) Local variation of the geomagnetic field during the filling of a reservoir. Geomagn Aeronomy 19(2):204–206

Ahmad MU (1964) A laboratory study of streaming potentials. Geophys Prospect 12:49–64

Aizawa K (2004) A large self-potential anomaly and its changes on the quiet Mt. Fuji, Japan. Geophys Res Lett 31:L05612, doi:10.1029/2004GL019462

Aizawa K, Yoshimura R, Oshiman N et al (2005) Hydrothermal system beneath Mt. Fuji volcano inferred from magnetotellurics and electric self-potential. Earth Planet Sc Lett 235(1–2):343–355

Aki K, Richards PG (1980) Quantitative seismology, theory and methods, vol. 1. W. H. Freeman and Company, New York

Avdeev DB (2005) Three-dimensional electromagnetic modelling and inversion from theory to application. Surv Geophys 26(6):767–799

Bahr K (1988) Interpretation of the magnetotelluric impedance tensor: regional induction and local telluric distortion. J Geophys 62:119–127

Bahr K (2000) Percolation in the crust derived from distortion of electric fields. Geophys Res Lett 27:1049–1052

Bahr K, Smirnov M, Steveling E et al (2002) A gelation analogy of crustal formation derived from fractal conductive structures. J Geophys Res 107(B11):2314, doi:10.1029/2001JB000506

Bakun WH (1987) Parkfield, California, earthquake prediction scenarios and response plans. U. S. Geological Survey Open File Report, 87–92

Bakun WH, Aagaard B, Dost B et al (2005) Implications for prediction and hazard assessment from the 2004 Parkfield earthquake. Nature 437(7061):969–974

Banks PO, Stacey FD, Liu SW (1991) Piezomagnetic fields of screw dislocation fault. J Geophys Res 96:21575–21582

Beamish D (1999) Characteristics of near surface electrokinetic coupling. Geophys J Int 137:231–242

Bernard P (1992) Plausibility of long distance electrotelluric precursors to earthquakes. J Geophys Res 97:17531–17546

Biagi PF, Kingsley SP, Vallianatos F (2000) Earthquake precursors. Phys Chem Earth 25(3):225

Biot MA (1956) Theory of propagation of elastic waves in a fluid-saturated porous solid 1 low-frequency range. J Acoust Soc Am 28:168–178

Bishop JR (1981) Piezoelectric effects on quartz-rich rocks. Tectonophysics 77:297–321

Blakely RJ (1995) Potential theory in gravity and magnetic applications. Cambridge University Press, Cambridge, UK

Brace WF, Orange AS (1968a) Electrical resistivity changes in saturated rocks during fracture and sliding. J Geophys Res 73:1433–1445
Brace WF, Orange AS (1968b) Further studies of the effects of pressure on electrical resistivity of rocks. J Geophys Res 73:5407–5420
Brennan BJ, Hastie LM (1979) Piezomagnetic effect of ground loading by lake Gordon, Tasmania. Tectonophysics 56:T9–T16
Butler KE, Russel RD, Kepic AW et al (1996) Measurements of the seismic response from a shallow boundary. Geophysics 61:1769–1778
Byrdina S, Friedel S, Wassermann J et al (2003) Self-potential variations associated with ultra-long-period seismic signals at Merapi volcano. Geophys Res Lett 30(22):2156, doi:10.1029/2003GL018272
Caldwell TG, Bibby HM, Brown C (2004) The magnetotelluric phase tensor. Geophys J Int 158(2):457–469
Campbell WH (1986) An interpretation of induced electric currents in long pipelines caused by natural geomagnetic sources of the upper-atmosphere. Surv Geophys 8(3):239–259
Chave AD, Smith JT (1994) On electric and magnetic galvanic distortion tensor decompositions. J Geophys Res 99(B3):4669–4682
Chave AD, Thomson DJ, Ander ME (1987) On the robust estimation of power spectra, coherences, and transfer-functions. J Geophys Res-Solid 92(B1):633–648
Chirkov YB (2004) The study of local sources of ULF geoelectric signals with steep fronts. Ann Geophys 47(1):213–227
Chu JJ, Gui X, Dai J et al (1996) Geoelectric signals in China and the earthquake generation process. J Geophys Res 101(B6):13869–13882
Corwin RF, Hoover DB (1979) The self-potential method in geothermal exploration. Geophysics 44:226–245
Currenti G, Del Negro C, Nunnari G (2005) Inverse modelling of volcanomagnetic fields using a genetic algorithm technique. Geophys J Int 163(1):403–418
Davis PM, Johnston MJS (1983) Localized geomagnetic field changes near active faults in California 1974–1980. J Geophys Res 88:9452–9460
Davis PM, Stacey FD (1972) Geomagnetic anomalies caused by a man-made lake. Nature 240:348–349
deGroot-Hedlin C (1991) Removal of static shift in two dimensions by regularized inversion. Geophysics 56:2102–2106
Del Negro C, Currenti G (2003) Volcanomagnetic signals associated with the 2001 flank eruption of Mt. Etna (Italy). Geophys Res Lett 30(7):1357, doi:10.1029/2002GL015481
Del Negro C, Ferrucci F (1998) Magnetic history of a dyke on Mount Etna (Sicily). Geophys J Int 133(2):451–458
Del Negro C, Ferrucci F (2000) Volcanomagnetic effects at Vulcano Island (Aeolian archipelago, Italy). Geophys J Int 140(1):83–94
Del Negro C, Currenti G, Napoli R et al (2004) Volcanomagnetic changes accompanying the onset of the 2002–2003 eruption of Mt. Etna (Italy). Earth Planetary Sci Lett 229(1–2):1–14
Dietrich JH (1992) Earthquake nucleation on faults with rate- and state-dependent strength. Tectonophysics 211:115–134
Egbert G, Booker JR (1986) Robust estimation of geomagnetic transfer functions. Geophys J R Astron Soc 87:173–194
Egbert GD, Booker JR (1992) Very long period magnetotellurics at tucson-observatory—implications for mantle conductivity. J Geophys Res-Solid 97(B11):15099–15112
Egbert GD, Booker JR, Schultz A (1992) Very long period magnetotellurics at tucson-observatory—estimation of impedances. J Geophys Res-Solid 97(B11):15113–15128
Enomoto Y, Zheng Z (1998) Possible evidences of earthquake lightning accompanying the 1995 Kobe earthquake inferred from the Nojima fault gouge. Geophys Res Lett 25(14):2721–2724
Fenoglio MA, Johnston MJS, Byerlee JD (1995) Magnetic and electric-fields associated with changes in high pore pressure in fault zones—application to the Loma-Prieta Ulf Emissions. J Geophys Res-Solid 100(B7):12951–12958
Ferré EC, Zechmeister MS, Geissman JW et al (2005) The origin of high magnetic remanence in fault pseudotachylytes: theoretical considerations and implication for coseismic electrical currents. Tectonophysics 402:125–139
Fraser-Smith AC, Bernardi A, McGill PR et al (1990) Low-frequency magnetic field measurements near the epicenter of the Ms7.1 Loma Prieta Earthquake. Geophys Res Lett 17:1465–1468
Freund F (2000) Time-resolved study of charge generation and propagation in igneous rocks. J Geophys Res 105:11001–11019
Freund F (2002) Charge generation and propagation in igneous rocks. J Geodyn 33:543–570
Friedel S, Byrdina S, Jacobs F et al (2004) Self-potential and ground temperature at Merapi volcano prior to its crisis in the rainy season of 2000–2001. J Volcanol Geotherm Res 134(3):149–168

Frost BR, Fyfe WS, Tazaki K et al (1989) Grain-boundary graphite in rocks and implications for high electrical conductivity in the lower crust. Nature 340:134–136
Fujinawa Y, Takahashi K, Matsumoto T et al (2000) Electromagnetic field anomaly associated with the 1998 seismic swarm in Central Japan. Phys Chem Earth Pt A 25(3):247–253
Fujinawa Y, Matsumoto T, Takahashi K (2002) Modeling confined pressure changes inducing anomalous electromagnetic fields related with earthquakes. J Appl Geophys 49(1–2):101–110
Fukao Y, Widiyantoro S, Obayashi M (2001) Stagnant slabs in the upper and lower mantle transition region. Rev Geophys 39:291–323
Fukuchi T (2003) Strong ferrimagnetic resonance signal and magnetic susceptibility of the Nojima pseudotachylyte in Japan and their implication for coseismic electromagnetic changes. J Geophys Res 108(B6):2312, doi:10.1029/2002JB002007
Garambois S, Dietrich M (2001) Seismo-electric wave conversion in porous media: field measurements and transfer function analysis. Geophysics 66:1417–1430
Garambois S, Dietrich M (2002) Full waveform numerical simulations of seismoelectromagnetic wave conversions in fluid-saturated stratified porous media. J Geophys Res-Solid 107(B7):2148, 10.1029/2001JB000316
Glover PWJ, Gomez JB, Meredith PG (2000a) Fractures in saturated rocks undergoing triaxial deformation using complex electrical measurements. Earth Planet Sci Lett 183:201–213
Glover PWJ, Hole PJ, Pous J (2000b) A modified Archie's law for two conducting phases. Earth Planet Sci Lett 180:369–383
Groom RW, Bahr K (1992) Corrections for near surface effects: decomposition of the magnetotelluric impedance tensor and scaling corrections for regional resistivities: a tutorial. Surv Geophys 13:341–379
Groom RW, Bailey RC (1989) Decomposition of magnetotelluric impedance tensors in the presence of local three-dimensional galvanic distortions. J Geophys Res 94:1913–1925
Gruszow S, Rossignol JC, Tzanis A et al (1996) Identification and analysis of electromagnetic signals in Greece: the case of the Kozani earthquake VAN prediction. Geophys Res Lett 23(16):2025–2028
Guichet X, Jouniaux L, Pozzi JP (2003) Streaming potential of a sand column in partial saturation conditions. J Geophys Res-Solid 108(B3):2141, doi:10.1029/2001JB001517
Haartsen MW, Pride S (1997) Electroseismic waves from point sources in layered media. J Geophys Res 102:24745–24769
Hamano Y (1983) Experiments on the stress sensitivity of natural remanent magnetization. J Geomagnet Geoelectr 35:155–172
Hanekop O, Simpson F (2006) Error propagation in electromagnetic transfer functions: what role for the magnetotelluric method in detecting earthquake precursors? Geophys J Int 165:763–774
Hao JQ, Hastie LM, Stacey FD (1982) Theory of the seismomagnetic effect: a reassessment. Phys Earth Planet Interior 28:129–140
Harinarayana T, Zlotnicki J (2006) Special issue of journal of applied geophysics "electrical and electromagnetic studies in geothermally active regions". J Appl Geophys 58:263–264
Hase H, Ishido T, Takakura S et al (2003) Zeta potential measurement of volcanic rocks from Aso caldera. Geophys Res Lett 30(23):2210, doi:10.1029/2003GL018694
Hase H, Hashimoto T, Sakanaka S et al (2005) Hydrothermal system beneath Aso volcano as inferred from self-potential mapping and resistivity structure. J Volcanol Geotherm Res 143(4):259–277
Hashimoto T, Tanaka Y (1995) A large self-potential anomaly on Unzen Volcano, Shimabara Peninsula, Kyushu Island, Japan. Geophys Res Lett 22:191–194
Hashimoto T, Tanaka Y, Johnston MJS et al (2003) On the annual variations on geomagnetic differences observed in Long Valley Caldera, California. Annuals of the Disaster Prevention Research Institute, Kyoto University 46 B:765–777 (in Japanese with English abstracts)
Hattori K, Serita A, Gotoh K et al (2004) ULF geomagnetic anomaly associated with 2000 Izu Islands earthquake swarm, Japan. Phys Chem Earth 29(4–9):425–435
Hautot S (2005) Modeling temporal variations of electrical resistivity associated with pore pressure change in a kilometer-scale natural system. Geochem Geophys Geosyst 6(6):Q06005, doi:10.1029/2004GC000859
Hautot S, Tarits P (2002) Effective electrical conductivity of 3-D heterogeneous porous media. Geophys Res Lett 29(14):1669, doi:10.1029/2002GL014907
Hautot S, Tarits P, Perrier F et al (2002) Groundwater electromagnetic imaging in complex geological and topographical regions: a case study of a tectonic boundary in the French Alps. Geophysics 53:967–978
Hayakawa M (ed) (1999) Atmospheric and ionospheric electromagnetic phenomena associated with earthquakes. Terra Scientific Publishing Co., Tokyo, Japan
Hayakawa M, Molchanov OA (eds) (2002) Seismoelectromagnetics (Lithosphere–Atmosphere–Ionosphere Coupling). Terra Scientific Publishing Co., Tokyo, Japan

Hayakawa M, Molchanov O A, Biagi P et al (2004) Preface. Phys Chem Earth 29:287
Honkura Y, Matsushima M, Oshiman N et al (2002) Small electric and magnetic signals observed before the arrival of seismic wave. Earth Planets Space 54(12):E9–E12
Hopkinson J (1889) Magnetic and other physical properties of iron at a high temperature. Philos Trans R Soc 46:443–465
Hoversten GM, Becker A (1995) EM1DSH with EMMODEL a Motif GUI, numerical modeling of multiple thin 3D sheets in a layered earth, University of California at Berkeley, Engineering Geoscience Department, Jun 12, 1995, and references therein
Hurst AW, Rickerby PC, Scott BJ et al (2004) Magnetic field changes on White Island, New Zealand, and the value of magnetic changes for eruption forecasting. J Volcanol Geotherm Res 136(1–2):53–70
Ichiki M, Uyeshima M, Utada H et al (2001) Upper mantle conductivity structure of the back-arc region beneath northeastern China. Geophys Res Lett 28(19):3773–3776
Ichiki M, Baba K, Obayashi M et al (2006) Water content and geotherm in the upper mantle above the stagnant slab: interpretation of electrical conductivity and seismic P-wave velocity models. Phys Earth Planet Interior 155(1–2):1–15
Ikeda T (1990) Fundamentals of piezoelectricity. Oxford University Press, Oxford, UK
Ishido T (2004) Electrokinetic mechanism for the "W"-shaped self-potential profile on volcanoes. Geophys Res Lett 31(15):L15616, doi:10.1029/2004GL020409
Ishido T, Mizutani H (1981) Experimental and theoretical basis of electrokinetic phenomena in rock-water systems and its applications to geophysics. J Geophys Res 86(NB3):1763–1775
Ishido T, Pritchett JW (1999) Numerical simulation of electrokinetic potentials associated with subsurface fluid flow. J Geophys Res-Solid 104(B7):15247–15259
Ishikawa N, Hashimoto M (1999) Average horizontal crustal strain rates in Japan during interseismic period deduced from geodetic surveys (Part 2). Zisin (J Seismol Soc Jpn) 52:299–315 (in Japanese with English abstracts)
Johnston MJS (1997) Review of electric and magnetic fields accompanying seismic and volcanic activity. Surv Geophys 18(5):441–475
Johnston MJS, Mueller RJ, Sasai Y (1994) Magnetic-field observations in the near-Field the 28 June 1992 M(W) 7.3 Landers, California, Earthquake. Bull Seismol Soc Am 84(3):792–798
Johnston MJS, Byerlee JD, Lockner D (2001) Rapid fluid disruption: a source for self-potential anomalies on volcanoes. J Geophys Res 106(B3):4327–4335
Johnston MJS, Byerlee JD, Lockner D (2002) Reply to comment by Revil on "Rapid fluid disruption: a source for self-potential anomalies on volcanoes" by M. J. S. Johnston, J. D. Byerlee, and D. Lockner. J Geophys Res 107(B8):2159, 10.1029/2002JB001794
Jones AG (1988) Static shift of magnetotelluric data and its removal in a sedimentary basin environment. Geophysics 53:967–978
Jouniaux L, Pozzi JP (1995) Streaming potential and permeability of saturated sandstones under triaxial stress: consequences for electrotelluric anomalies prior to earthquakes. J Geophys Res 100:10197–10209
Kagiyama T, Utada H, Yamamoto T (1999) Magma ascent beneath Unzen Volcano, SW Japan, deduced from the electrical resistivity structure. J Volcanol Geotherm Res 89(1–4):35–42
Kalashnikov AG, Kapista SP (1952) Magnetic susceptibility of rocks under mechanical stresses. Dokl Akad Nauk USSR 86:521–523
Kanda W, Uyeshima M, Makris J et al (2000) Electric field polarization around Ioannina VAN station, Greece, inferred from a resistivity mapping. Phys Earth Planet Interior 119(3–4):269–283
Kariya KA, Shankland TJ (1983) Electrical conductivity of dry lower crustal rocks. Geophysics 48:52–61
Kinoshita M, Uyeshima M, Uyeda S (1989) Earthquake prediction research by means of telluric potential monitoring, Progress Report No. 1: installation of monitoring network. Bull Earthq Res I Tokyo 64:255–311
Kiss J, Szarka L, Prácser E (2005) Second-order magnetic phase transition in the Earth. Geophysical Research Letters 32:L24310, doi:10.1029/2005GL024199
Kondo S, Uyeda S, Nagao T (2002) The selectivity of the Ioannina VAN station. J Geodyn 33:433–461
Kumagai H, Ohminato T, Nakano M et al (2001) Very-long-period seismic signals and caldera formation at Miyake Island, Japan. Science 293:687–690
Langbein J, Borcherdt R, Dreger D et al (2005) Preliminary report on the 28 September 2004, M 6.0 Parkfield, California earthquake. Seismol Res Lett 76(1):10–26
Lazarus D (1996) Physical mechanisms for generation and propagation of seismic electric signals. In: Lighthill Sir J (ed) A critical review of VAN: earthquake prediction from seismic electric signals. World Scientific, Singapore, pp 91–96
Lewicki JL, Connor C, St-Amand K et al (2003) Self-potential, soil CO2 flux, and temperature on Masaya volcano, Nicaragua. Geophys Res Lett 30(15):1817, doi:10.1029/2003GL017731

Lorne B, Perrier F, Avouac JP (1999) Streaming potential measurements 2. Relationship between electrical and hydraulic flow patterns from rock samples during deformation. J Geophys Res-Solid 104(B8):17879–17896

Madden TR (1983) High sensitivity monitoring of resistivity and self potential variations in the Palmdale and Hollister areas for earthquake prediction studies. Final technical report, contract 14-08-0001-19249, U.S. Geol Surv, Reston, Va

Madden TR, LaTorraca GA, Park SK (1993) Electrical conductivity variations around the Palmdale section of the San Andreas Fault Zone. J Geophys Res 98:795–808

Marquis G, Darnet M, Sailhac P et al (2002) Surface electric variations induced by deep hydraulic stimulation: an example from the Soultz HDR site. Geophys Res Lett 29(14):1662, 10.1029/2002GL015046

Martí A, Queralt P, Jones AG, Ledo J (2005) Improving Bahr's invariant parameters using the WAL approach. Geophys J Int 163:38–41

Maruyama T (1964) Statical elastic dislocations in an infinite and semi-infinite medium. Bull Earthq Res I Tokyo 42:289–368

Matsushima M, Honkura Y, Oshiman N et al (2002) Seismoelectromagnetic effect associated with the Izmit earthquake and its aftershocks. Bull Seismol Soc Am 92(1):350–360

Merill RT, McElhinny MW, McFadden PL (1996) The magnetic field of the earth: paleomagnetism, the core, and the deep mantle. International geophysics series. Adademic Press, Inc., San Diego, USA

Michel S, Zlotnicki J (1998) Self-potential and magnetic surveying of La Fournaise volcano (Réunion Island): correlations with faulting, fluid circulation, and eruption. J Geophys Res 103:17845–17857

Mikhailov OV, Haartsen MW, Toksoz MN (1997) Electroseismic investigation of the shallow subsurface: field measurements and numerical modeling. Geophysics 62:97–105

Mikhailov OV, Queen JH, Toksoz MN (2000) Using borehole electroseismic measurements to detect and characterize fractured (permeable) zones. Geophysics 65:1098–1112

Mizutani H, Ishido T (1976) New interpretation of magnetic-field variation associated with Matsushiro earthquakes. J Geomagnet Geoelectr 28(2):179–188

Mizutani H, Ishido T, Yokokura T et al (1976) Electrokinetic phenomena associated with earthquakes. Geophys Res Lett 3(7):365–368

Mogi K (1958) Relations between the eruptions of various volcanoes and the deformations of the ground surfaces around them. Bull Earthq Res I Tokyo 36:99–134

Mori T (1985) A test observation of geoelectric field with a long electrode span. Pap Meteorol Geophys 36:149–155 (in Japanese)

Mori T (1987) Variations in the geoelectric field with relation to crustal conditions of the earth. Geophys Mag 42:41–104

Morrow C, Brace WF (1981) Electrical resistivity changes in tuffs due to stress. J Geophys Res 86:2929–2934

Murakami H, Hashimoto T, Oshiman N et al (2001) Electrokinetic phenomena associated with a water injection experiment at the Nojima fault on Awaji Island, Japan. Island Arc 10(3–4):244–251

Nagao T, Uyeda S, Asai Y et al (1996) Anomalous changes in geoelectric potential preceding four earthquakes in Japan. In: Lighthill Sir J (ed) A critical review of VAN. World Scientific, Singapore, pp 292–300

Nagao T, Orihara Y, Yamaguchi T et al (2000) CoseismicCoseismic geoelectric potential changes observed in Japan. Geophys Res Lett 27(10):1535–1538

Nagata T (1943) The natural remanent magnetism of volcanic rocks and its relation to geomagnetic phenomena. Bull Earthq Res I Tokyo 21:1–196

Nagata T (1970) Basic magnetic properties of rocks under the effect of mechanical stresses. Tectonophysics 9:167–195

Nakamura N, Hirose T, Borradaile J (2002) Laboratory verification of submicron magnetic production in pseudotachylytes: relevance for paleointensity studies. Earth Planet Sci Lett 201:13–18

Neal SL, Mackie RL, Larsen JC et al (2000) Variations in the electrical conductivity of the upper mantle beneath North America and the Pacific Ocean. J Geophys Res-Solid 105(B4):8229–8242

Néel L (1949) The'orie du trainage magne'tizue des ferromagne'tiques aux grains fins avec applications aux terres cuites. Ann Geophys 5:99–136

Nesbitt BE (1993) Electrical resistivities of crustal fluids. J Geophys Res 98:4301–4310

Nishida Y, Sugisaki Y, Takahashi K et al (2004) Tectonomagnetic study in the eastern part of Hokkaido, NE Japan: discrepancy between observed and calculated results. Earth Planets Space 56(11):1049–1058

Nitsan U (1977) Electromagnetic emmision accomapanying fracture of quartz-bearing rocks. Geophys Res Lett 4:333–336

Ogawa Y (2002) On two-dimensional modeling of magnetotelluric field data. Surv Geophys 23(2–3):251–273

Ogawa Y, Uchida T (1996) A two-dimensional magnetotelluric inversion assuming Gaussian static shift. Geophys J Int 126:69–76
Ogawa T, Utada H (2000a) Coseismic piezoelectric effects due to a dislocation—1. An analytic far and early-time field solution in a homogeneous whole space. Phys Earth Planet Interior 121(3–4):273–288
Ogawa T, Utada H (2000b) Electromagnetic signals related to incidence of a teleseismic body wave into a subsurface piezoelectric body. Earth Planets Space 52(4):253–260
Ohnaka M (1992) Earthquake source nucleation: a physical model for short-term precursors. Tectonophysics 211:149–178
Okada Y (1992) Internal deformation due to shear and tensile faults in a half-space. Bull Seismol Soc Am 82:1018–1992
Okubo A, Oshiman N (2004) Piezomagnetic field associated with a numerical solution of the Mogi model in a non-uniform elastic medium. Geophys J Int 159(2):509–520
Oshiman N, Sasai Y, Miyakoshi J et al (1991) Continuous observation of piezomagnetic changes due to ground loading by Lake Nichinan, Tottori, Japan. Proceedings of Conductivity Anomaly Symposium (1991):137–148 (in Japanese)
Overbeek JThG (1952) In: Kruyt HR (ed) Irreversible systems, colloid science, vol. 1, Elsevier, New York, 389 pp
Park SK (1991) Monitoring changes of resistivity prior to earthquakes in Parkfield, California with telluric arrays. J Geophys Res 96:14211–14237
Park SK (1996) Precursors to earthquakes: seismoelectromagnetic signals. Surv Geophys 17(4):493–516
Park SK (1997) Monitoring resistivity changes in Parkfield, California: 1988–1995. J Geophys Res 102:24545–24559
Park SK (2002) Perspectives on monitoring resistivity changes with telluric signals at Parkfield, Calfornia: 1988–1999. J Geodyn 33:379–399
Park SK, Fitterman DV (1990) Sensitivity of the telluric monitoring array in Parkfiekd, California to changes of resistivity. J Geophys Res 95:15557–15571
Park SK, Johnston MJS, Madden TR et al (1993) Electromagnetic precursors in the ULF band: a review of observations and mechanisms. Rev Geophys 31:117–132
Parker RL, Booker JR (1996) Optimal one-dimensional inversion and bounding of apparent resistivity and phase measurement. Phys Earth Planet Interior 98:269–282
Parks GA (1965) The isoelectric points of solid oxides, solid hydroxides, and aqueous hydroxo complex systems. Chem Rev 65:177–198
Parrot M (2006) Preface special issue of planetary and space science 'DEMETER'. Planet Space Sci 54:411–412
Perrier F, Trique M, Lorne B et al (1998) Electric potential variations associated with yearly lake level variations. Geophys Res Lett 25(11):1955–1958
Perrier F, Trique M, Aupiais J et al (1999) Electric potential variations associated with periodic spring discharge in western Nepal. CR Acad Sci II A 328(2):73–79
Perrier F, Morat P, Yoshino T et al (2004) Seasonal thermal signatures of heat transfer by water exchange in an underground vault. Geophys J Int 158:372–384
Pham VN, Boyer D, Chouliaras G et al (1998) Characteristics of electromagnetic noise in the Ioannina region (Greece); a possible origin for so called "Seismic Electric Signal" (SES). Geophys Res Lett 25(12):2229–2232
Pham VN, Boyer D, Le Mouel JL et al (1999) Electromagnetic signals generated in the solid Earth by digital transmission of radio-waves as a plausible source for some so-called 'seismic electric signals'. Phys Earth Planet Interior 114(3–4):141–163
Pham VN, Boyer D, Perrier F et al (2001) Generation mechanisms of telluric noises in ULF band: possible sources for the so-called 'seismic electric signals' (SES). CR Acad Sci II A 333(5):255–262
Pham VN, Boyer D, Chouliaras G et al (2002) Sources of anomalous transient electric signals (ATESs) in the ULF band in the Lamia region (central Greece): electrochemical mechanisms for their generation. Physics Earth Planet Interior 130(3–4):209–233
Pinettes P, Bernard P, Cornet F et al (2002) On the difficulty of detecting streaming potentials generated at depth. Pure Appl Geophys 159(11–12):2629–2657
Pride S (1994) Governing equations for the coupled electromagnetics and acoustics of porous media. Phys Rev B 50(21):15678–15696
Reppert PM, Morgan FD (2003a) Temperature-dependent streaming potentials: 1. Theory. J Geophys Res-Solid 108(B11):2546, doi:10.1029/2002JB001754
Reppert PM, Morgan FD (2003b) Temperature-dependent streaming potentials: 2. Laboratory. J Geophys Res-Solid 108(B11):2547, doi:10.1029/2002JB001755

Revil A (2002) Comment on "Rapid fluid disruption: a source for self-potential anomalies on volcanoes" by M. J. S. Johnston, J. D. Byerlee, and D. Lockner. J Geophys Res 107(B8):2155, doi:10.1029/2001JB000788
Revil A, Pezard PA, Glover PWJ (1999a) Streaming potential in porous media 1. Theory of zeta potentials. J Geophys Res-Solid 104(B9):20021–20032
Revil A, Schwaeger H, Cathles LM et al (1999b) Streaming potential in porous media 2. Theory and application to geothermal systems. J Geophys Res-Solid 104(B9):20033–20048
Revil A, Finizola A, Sortino F et al (2004) Geophysical investigations at Stromboli volcano, Italy: implications for ground water flow and paroxysmal activity. Geophys J Int 157(1):426–440
Rikitake T, Yamazaki Y (1976) Resistivity changes as a precursor of earthquake. J Geomagnet Geoelectr 28(6):497–505
Rizzo E, Suski B, Revil A et al (2004) Self-potential signals associated with pumping tests experiments. J Geophys Res-Solid 109(B10):B10203, doi:10.1029/2004JB003049
Roberts J, Duba A, Mathez E et al (1999) Carbon enhanced electrical conductivity during fracture of rocks. J Geophys Res 104:737–747
Roder H, Buttner R, Zimanowski B (2002) Seismo-electrical effects: experiments and field measurements. Appl Phys Lett 80(2):doi: 10.1063/1.1431693
Rooney WJ (1949) Earth-current results at tucson magnetic observatory, 1932–1942. Res Dep of Terr Magn Carnegie Inst Washington, 9, 307 pp
Russel RD, Butler KE, Kepic AW et al (1997) Seismoelectric exploration. Leading Edge 16:1611–1615
Sagiya T, Miyazaki S, Tada T (2000) Continuous GPS array and present-day crustal deformation of Japan. Pure Appl Geophys 157:2303–2322
Sakanaka S, Oshiman N, Sumitomo N (1997) A hybrid calculation method of tectonomagnetic effect using BEM and the surface integral representation of the piezomagnetic potential—two dimensional case study. J Geomagnet Geoelectr 49(1):101–118
Sarlis N, Lazaridou M, Kapiris P et al (1999) Numerical model of the selectivity effect and the Delta V/L criterion. Geophys Res Lett 26(21):3245–3248
Sasai Y (1980) Application of the elasticity theory of dislocations to tectonomagnetic modeling. Bull Earthq Res I Tokyo 55:387–447
Sasai Y (1991) Tectonomagnetic modeling on the basis of the linear piezomagnetic effect. Bull Earthq Res I Tokyo 66:585–722
Sasai Y (1994) Piezomagnetic fields produced by dislocation sources. Surv Geophys 15(4):363–382
Sasai Y (2001) Tectonomagnetic modeling based on the piezomagnetism: a review. Annali Di Geofisica 44(2):361–368
Sasai Y, Ishikawa Y (1997) Seismomagnetic models for earthquakes in the eastern part of Izu Peninsula, Central Japan. Annali Di Geofisica 40(2):463–478
Sasai Y, Zlotnicki J, Nishida Y et al (1997) Electromagnetic monitoring of Miyake-jima volcano, Izu-Bonin Arc, Japan: a preliminary report. J Geomagnet Geoelectr 49(11–12):1293–1316
Sasai Y, Uyeshima M, Utada H et al (2001a) The 2000 activity of Miyake-jima volcano as inferred from electric and magnetic field observations. J Geogr 110:226–244 (in Japanese with English abstracts)
Sasai Y, Zlotnicki J, Nishida Y et al (2001b) Evaluation of electric and magnetic field monitoring of Miyake-jima volcano (Central Japan): 1995–1999. Annali Di Geofisica 44(2):239–260
Sasai Y, Uyeshima M, Zlotnicki J et al (2002) Magnetic and electric field observations during the 2000 activity of Miyake-jima volcano, Central Japan. Earth Planet Sci Lett 203(2):769–777
Satoh H, Nishida Y, Ogawa Y et al (2001) Crust and upper mantle resistivity structure in the southwestern end of the Kuril Arc as revealed by the joint analysis of conventional MT and network MT data. Earth Planets Space 53(8):829–842
Scholz CH, Sykes LR, Aggraval YP (1973) Earthquake prediction—a physical basis. Science 181:803–810
Shiozaki I, Nishigaki T, Oshiman N et al (1999) Preliminary report on the resistivity structure derived from the Network MT investigation in the eastern part of Chugoku district, southwestern Honshu, Japan. Rep Fac Eng Tottori Univ 30:49–60 (in Japanese with English abstract)
Simpson JJ, Taflove A (2005) Electrokinetic effect of the Loma Prieta earthquake calculated by an entire-Earth FDTD solution of Maxwell's equations. Geophys Res Lett 32(9):L09302, doi:10.1029/2005GL022601
Singer BS (1992) Correction for distortions of magnetotelluric fields: limits of validity of the static approach. Surv Geophys 13:309–340
Siripunvaraporn W, Egbert G (2000) An efficient data-subspace inversion method for 2-D magnetotelluric data. Geophysics 65:791–803
Siripunvaraporn W, Uyeshima M, Egbert G (2004) Three-dimensional inversion for Network-Magnetotelluric data. Earth Planets Space 56(9):893–902

Siripunvaraporn W, Egbert G, Lenbury Y et al (2005) Three-dimensional magnetotelluric inversion: data-space method. Phys Earth Planet Interior 150(1–3):3–14
Skordas E, Kapiris P, Bogris N et al (2000) Field experimentation on the detectability of coseismiccoseismic electric signals. Proc Jpn Acad B-Phys 76(4):51–56
Slifkin L (1993) Seismic electric signals displacement of charged dislocation. Tectonophysics 224:149–152
Slifkin L (1996) A dislocation model for seismic electric signals. In: Lighthill Sir J (ed) A critical review of VAN: earthquake prediction from seismic electric signals. World Scientific, Singapore, pp 97–104
Spitzer K (1995) A 3D finite difference algorithm for DC resistivity modeling using conjugate gradient methods. Geophys J Int 123:903–914
Stacey FD (1964) The seismomagnetic effect. Pure Appl Geophys 97:146–155
Stavrakas I, Anastasiadis C, Triantis D et al (2003) Piezo stimulated currents in marble samples: precursory and concurrent-with-failure signals. Nat Hazards Earth Syst Sci 3:243–247
Stuart WD, Banks PO, Sasai Y et al (1995) Piezomagnetic field for Parkfield fault model. J Geophys Res 100(B12):24101–24110
Sumitomo N, Oshiman N, Sakanaka S et al (1997) Tectonoelectric signal related with the occurrence of the 1995 Hyogo-ken Nanbu earthquake (M7.2) and preliminary results of electromagnetic observation around the focal area. J Phys Earth 45(2):91–104
Takeuchi A, Nagahama H (2002a) Interpretation of charging on fracture or frictional slip surface of rocks. Phys Earth Planet Interior 130:285–291
Takeuchi A, Nagahama H (2002b) Surface charging mechanism and scaling law related to earthquakes. J Atmos Electr 22:183–190
Tanaka Y (1993) Eruption mechanism as inferred from geomagnetic changes with special attention to the 1989–1990 activity of Aso volcano. J Volcanol Geotherm Res 56(3):319–338
Tarits P, Hautot S, Perrier F (2004) Water in the mantle: results from electrical conductivity beneath the French Alps. Geophys Res Lett 31:L06612, doi:10.1029/2003GL019277
Teisseyer R (2001) Dislocation dynamics and related electromagnetic excitation. Acta Geophys Pol 49:55–73
Torres-Verdin C, Bostick FX (1992a) Implications of the Born approximation for the magnetotelluric problem in three-dimensional environments. Geophysics 57:587–602
Torres-Verdin C, Bostick FX (1992b) Principles of spatial surface electric field filtering in magnetotellurics: electromagnetic array profiling (EMAP). Geophysics 57:603–622
Tosha T, Matsushima N, Ishido T (2003) Zeta potential measured for an intact granite sample at temperatures to 200 degrees C. Geophys Res Lett 30(6):1295, doi:10.1029/2002GL016608
Tournerie B, Chouteau M (1998) Deep Conductivity Structure in Abitibi, Canada, using Long Dipole Magnetotelluric Measurements. Geophys Res Lett 25(13):2317–2320
Trique M, Richon P, Perrier F et al (1999) Radon emanation and electric potential variations associated with transient deformation near reservoir lakes. Nature 399(6732):137–141
Trique M, Perrier F, Froidefond T et al (2002) Fluid flow near reservoir lakes inferred from the spatial and temporal analysis of the electric potential. J Geophys Res-Solid 107(B10):2239, doi:10.1029/2001JB000482
Tuck GJF, Stacey FD, Starkey A (1977) A search for the piezoelectric effect in quartz-bearing rocks. Tectonophysics 39:T7–T11
Tyburczy JA, Waff HS (1983) Electrical conductivity of molten basalt and andesite to 25 kilobar pressure—Geophysical significance and implications of geophysical research. J Geophys Res 88:2413–2430
Ukawa M, Fujita E, Yamamoto E et al (2000) The 2000 Miyakejima eruption crustal deformation and earthquakes observed by NIED Miyakejima observation network. Earth Planets Space 52:19–26
Utada H (2003) Interpretation of time changes in the apparent resistivity observed prior to the 1986 eruption of Izu-Oshima volcano, Japan. J Volcanol Geotherm Res 126:97–107
Utada H, Munekane H (2000) On galvanic distortions of regional 3-D MT impedances. Geophys J Int 140:385–398
Utada H, Yoshino T, Okubo T et al (1998) Seismic resistivity changes observed at Aburatsubo, central Japan, revisited. Tectonophysics 299(4):317–331
Utada H, Neki M, Kagiyama T (2000) A study of annual variations in the geomagnetic total intensity with special attention to detecting volcanomagnetic signals. Earth Planets Space 52(2):91–103
Utsugi M, Nishida Y, Sasai Y (2000) Piezomagnetic potentials due to an inclined rectangular fault in a semi-infinite medium. Geophys J Int 140(3):479–492
Uyeda S, Park S (2002) Preface. J Geodyn 33:377–378
Uyeda S, Nagao T, Orihara Y et al (2000) Geoelectric potential changes: possible precursors to earthquakes. Proc Natl Acad USA 97(9):4561–4566
Uyeda S, Hayakawa M, Nagao T et al (2002) Electric and magnetic phenomena observed before the volcano-seismic activity 2000 in the Izu Island Region, Japan. Proc Natl Acad USA 99(11):7352–7355

Uyeshima M, Kinoshita M, Iino H et al (1989) Earthquake prediction research by means of telluric potential monitoring, Progress Report No. 2: preliminary study on Teshikaga channel 2 signals and the seismicity in the region off Kushiro. Bull Earthq Res I Tokyo 64:487–515
Uyeshima M, Kanda W, Nagao T et al (1998). Directional properties of VAN's SES and ULF MT signals at Ioannina, Greece. Phys Earth Planet Interior 105(3–4):153–166
Uyeshima M, Utada H, Nishida Y (2001) Network-magnetotelluric method and its first results in central and eastern Hokkaido, NE Japan. Geophys J Int 146(1):1–19
Uyeshima M, Ichiki M, Fujii I et al (2002) Netowork-MT survey in Japan to determine nation-wide deep electrical conductivity structure. In: Fujinawa Y, Yoshida A (eds) Seismotectonics in convergent plate boundary. TERRAPUB, Tokyo, pp 107–121
Vallianatos F, Triantis D, Tzanis A et al (2004) Electric earthquake precursors: from laboratory results to field observations. Phys Chem Earth 29(4–9):339–351
Varotsos P (2005) The physics of seismic electric signals. TERRAPUB, Tokyo, Japan
Varotsos P, Alexopoulos K (1984a) Physical-properties of the variations of the electric-field of the earth preceding earthquakes.1. Tectonophysics 110(1–2):73–98
Varotsos P, Alexopoulos K (1984b) Physical-properties of the variations of the electric-field of the earth preceding earthquakes.2. Determination of Epicenter and Magnitude Tectonophysics 110(1–2):99–125
Varotsos P, Alexopoulos K (1986) Thermodynamics of point defects and their relation with bulk properties. North Holland, Amsterdam
Varotsos P, Bogris NG, Kyritsis A (1992) Comments on the depolarization currents stimulated by variations of temperature or pressure. J Phys Chem Solids 53(8):1007–1011
Varotsos P, Alexopoulos K, Lazaridou M (1993) Latest aspects of earthquake prediction in greece based on seismic electric signals.2. Tectonophysics 224(1–3):1–37
Varotsos P, Hadjicontis V, Nowick AS (2001) The physical mechanism of seismic electric signals. Acta Geophys Pol 49:415–421
Verier V, Rochette P (2002) Estimating peak currents at ground lightning impacts using remanent magnetization. Geophys Res Lett 29(18):1867, doi:10.1029/2002GL015207
Viljanen A, Pirjola R (1994) Geomagnetically induced currents in the finnish high-voltage power-system—geophysical review. Surv Geophys 15(4):383–408
Wannamaker PE, Stodt JA, Rijo L (1986) Two-dimensional topographic responses in magnetotelluric model using finite elements. Geophysics 51:2131–2144
Warwick JW, Stoker C, Meyer TR (1982) Radio emission associated with rock fracture: possible application to the great Chilean earthquake of May 22, 1960. J Geophys Res 87:2851–2859
Weaver JT, Agarwal AK, Lilley FEM (2000) Characterization of the magnetotelluric tensor in terms of its invariants. Geophys J Int 141:321–336
Wrumstich B, Morgan FD (1994) Modelling of streaming potential response by oil well pumping. Geophysics 59:46–56
Yamaguchi S, Kobayashi Y, Oshiman N et al (1999) Preliminary report on regional resistivity variation inferred from the Network MT investigation in the Shikoku district, southwestern Japan. Earth Planets Space 51(3):193–203
Yamazaki Y (1965) Electrical conductivity of saturated rocks (The 1st paper), Laboratory experiments on sedimentary rocks. Bull Earthq Res I Tokyo 43:783–802
Yamazaki Y (1966) Electrical conductivity of strained rocks (The 2nd paper), Further experiments on sedimentary rocks. Bull Earthq Res I Tokyo 44:1553–1570
Yamazaki Y (1967) Electrical conductivity of strained rocks (The 3rd paper), A resistivity variometer. Bulletin of the Earthquake Research Institute-University of Tokyo 45:849–860
Yamazaki Y (1975) Precursory and coseismic resistivity changes. Pure Appl Geophys 113(1–2):219–227
Yoshida S (2001) Convection current generated prior to rupture in saturated rocks. J Geophys Res-Solid 106(B2):2103–2120
Yoshida S, Ogawa T (2004) Electromagnetic emissions from dry and wet granite associated with acoustic emissions. J Geophys Res 109:B09204, doi:10.1029/2004JB003092
Yoshida S, Uyeshima M, Nakatani M (1997) Electric potential changes associated with slip failure of granite: preseismic and coseismic signals. J Geophys Res-Solid 102(B7):14883–14897
Yoshida S, Clint OC, Sammonds PR (1998) Electric potential changes prior to shear fracture in dry and saturated rocks. Geophys Res Lett 25:1577–1580
Yukutake T, Yoshino T, Utada H et al (1990) Changes in the electrical resistivity if the central cone, Mihara-yama, of Oshima Volcano observed by a direct current method. J Geomagnet Geoelectr 42:151–169
Zhan Z (1989) Investigations of tectonomagnetic phenomena in China. Phys Earth Planet Interior 57:11–22
Zhao Y, Qian F (1994) Geoelectric precursors to strong earthquakes in China. Tectonophysics 233:99–113

Zlotnicki J, Nishida Y (2003) Review on morphological insights of self-potential anomalies on volcanoes. Surveys in Geophysics 24(4):291–338
Zlotnicki J, Pozzi JK, Cornet FH (1981) Investigation of induced magnetization variations caused by triaxial stresses. J Geophys Res 86:11899–11909
Zlotnicki J, Michel S, Ammen C (1994) Anomalies de polarization spontanee et systems convectifs sur le volcan du Piton de la Gournaise (Ile de la Reunion, France). CR Acad Sci, Paris 318:1325–1331
Zlotnicki J, Sasai Y, Yvetot P et al (2003) Resistivity and self-potential changes associated with volcanic activity: the July 8, 2000 Miyake-jima eruption (Japan). Earth Planet Sci Lett 205(3–4):139–154
Zlotnicki J, Le Mouel JL, Kanwar R et al (2006). Ground-based electromagnetic studies combined with remote sensing based on Demeter mission: a way to monitor active faults and volcanoes. Planet Space Sci 54(5):541–557